AGU ADVANCING EARTH AND SPACE SCIENCE

Water Resources Research

RESEARCH ARTICLE
10.1029/2021WR031873

Bedload Fluxes in a Glacier-Fed River at Multiple Temporal Scales

Velio Coviello[1,2], Gianluca Vignoli[3,4], Silvia Simoni[5], Walter Bertoldi[6], Michael Engel[2], Anuschka Buter[2], Giulia Marchetti[2], Andrea Andreoli[2], Sara Savi[2,7], and Francesco Comiti[2]

[1]Research Institute for Geo-Hydrological Protection, CNR, Padova, Italy, [2]Faculty of Science and Technology, Free University of Bozen-Bolzano, Bozen-Bolzano, Italy, [3]CISMA Srl, Bozen-Bolzano, Italy, [4]Now at Penta Automazioni Industriali srl, Molinella, Italy, [5]Mountain-eering Srl, Bozen-Bolzano, Italy, [6]Dipartimento di Ingegneria Civile Ambientale e Meccanica, Università degli Studi di Trento, Trento, Italy, [7]Institute of Geosciences, University of Potsdam, Potsdam, Germany

Key Points:

- The power of the geophone-plate seismic signal better reflects the variability of bedload rate than the number of threshold-based impulses
- Highest bedload rates ($>10^3$ kg m^{-1} min^{-1}) produced by summer rainstorm events occur during snow- and glacier-melt periods
- Temperature-controlled glacier melt flows are most effective in transporting bedload, followed by rainfall-driven 1.5–2 years floods

Supporting Information:

Supporting Information may be found in the online version of this article.

Correspondence to:

V. Coviello,
velio.coviello@cnr.it

Citation:

Coviello, V., Vignoli, G., Simoni, S., Bertoldi, W., Engel, M., Buter, A., et al. (2022). Bedload fluxes in a glacier-fed river at multiple temporal scales. *Water Resources Research*, *58*, e2021WR031873. https://doi.org/10.1029/2021WR031873

Received 22 DEC 2021
Accepted 15 SEP 2022

Author Contributions:

Conceptualization: Velio Coviello, Francesco Comiti
Data curation: Velio Coviello, Gianluca Vignoli
Formal analysis: Velio Coviello
Funding acquisition: Gianluca Vignoli, Walter Bertoldi, Francesco Comiti
Investigation: Velio Coviello, Gianluca Vignoli, Silvia Simoni, Walter Bertoldi, Michael Engel, Giulia Marchetti
Methodology: Velio Coviello, Gianluca Vignoli, Silvia Simoni, Walter Bertoldi, Francesco Comiti

Abstract

In mountain rivers, long-term observations of water and sediment fluxes are crucial for understanding the dynamics of bedload fluctuations. We analyze 7 years of continuous data gathered from eight geophone plates at a monitoring station in the glacier-fed Sulden/Solda River (South Tyrol, Italy) to estimate the bedload flux at 1-min scale. Sixty-five bedload samples were used to derive the calibration equations adopted to quantify the transported bedload mass. The signal power is proposed as a more effective metric than threshold-based impulses for calculating bedload masses. Results show (a) a remarkable variability of bedload rates for the same value of flow discharge, (b) the joint effect of storm-driven flood events and seasonal changes in sediment supply on bedload rates, and (c) the strong impact of climatic factors (i.e., temperature and snow cover) on bedload fluxes. Moderate bedload rates occurring in late spring/early summer are likely related to the mobilization of riverbed sediments, while sustained bedload transport during melt flows in July–August—corresponding to the effective bedload discharge range—is associated with the activation of glacial and proglacial sediment sources. The data set shows a complex climatic control on bedload transport at the basin scale, where precipitation, air temperature, and snow cover determine flow and glacier melting dynamics. These findings suggest how the effects of climate change in the Alps likely will lead to an increase in peak bedload rates in a context of declining annual bedload yields as melt flows will progressively reduce in the next decades.

Plain Language Summary

Water flowing in mountain rivers can transport a large amount of bedload, which is the coarse sediments that jump and roll on the river bed. The knowledge of the bedload flux matters for both improved understanding of the ecosystem and of the effects of human activities. Measuring how much bedload is transported is difficult as particles move below the water level. In this study, we employ seismic sensors installed on the river bed to quantify bedload transported by an Alpine river originating from a glacierized area. Moving particles produce ground vibrations that are more intense when the river transports more material. We found that the intensity of bedload measured by this "seismic noise" is extremely variable during the year and controlled by weather conditions. In particular, the river can rapidly increase the transport of sediments during high runoff peaks induced by glacier melt and summer thunderstorms. These findings are particularly relevant in the context of ongoing global warming that is dramatically impacting mountain areas where newly exposed stream reaches are emerging from the rapidly melting glaciers.

1. Introduction

In mountain rivers, bedload transport is the main driver of erosional/depositional processes and understanding its dynamics is crucial for the conservation of fluvial ecosystems, flood risk mitigation, and hydropower management (Harrison et al., 2011; Lenzi et al., 2004; Rickenmann et al., 2016). The quantification of bedload fluxes is relevant for understanding both ecosystem functioning and the effects of human activities on rivers, but it is affected by large uncertainties. Traditional transport capacity-based equations assume that—at a given stable river cross section—bedload transport rates are a function of the excess of a driving flow variable (e.g., dimensionless shear stress, unit discharge, and unit stream power) with respect to the respective threshold value for sediment motion, which depends on both local flow and sediment properties (Bagnold, 1977; Einstein, 1950; Meyer-Peter & Müller, 1948). However, those equations are now known to largely overestimate the actual bedload rates in steep mountain rivers under ordinary flow conditions, due to both sediment supply limitations and form

Project Administration: Gianluca Vignoli, Francesco Comiti
Resources: Gianluca Vignoli, Silvia Simoni, Walter Bertoldi, Andrea Andreoli, Sara Savi
Software: Velio Coviello, Gianluca Vignoli
Supervision: Francesco Comiti
Validation: Velio Coviello, Michael Engel, Andrea Andreoli, Francesco Comiti
Writing – original draft: Velio Coviello
Writing – review & editing: Velio Coviello, Gianluca Vignoli, Silvia Simoni, Walter Bertoldi, Michael Engel, Giulia Marchetti, Andrea Andreoli, Sara Savi, Francesco Comiti

roughness (Barry et al., 2004; Comiti & Mao, 2012; Rickenmann, 2001; Schneider et al., 2016). Indeed, different sediment supply regimes, runoff origin, and history of flood events have a strong impact on bedload fluxes and make uncertainties in bedload prediction very large (Mao, 2012; Recking, 2012; Turowski et al., 2011).

Also, the long-established concept—initially proposed for low-gradient, transport-limited rivers—that ordinary floods (1–2 years recurrence interval) are most effective in transporting be sediments in the long-term than extreme, rare events (Wolman & Miller, 1960) has been challenged in steep channels (Bunte et al., 2014; Lenzi et al., 2006). Thanks to the long-term bedload transport data collected in the Rio Cordon (Italian Alps, characterized by a nivo-pluvial hydrological regime), the latter authors showed how a single value of bedload effective discharge may be not applicable in such systems, and that floods larger than "bankfull events" may exert a stronger role than in lowland rivers.

Long-term (i.e., multiannual) bedload monitoring is crucial to fill the large knowledge gaps still present about bedload dynamics, especially in supply limited mountain rivers. Bedload monitoring based on geophone plates has been developed and applied for many years in Austria and Switzerland (e.g., Habersack et al., 2017; Rickenmann et al., 2012). Generally, geophone-plate data are analyzed combined with direct bedload measurements to obtain calibration equations and to calculate bedload rates. Some information on the grain size distribution of bedload can be extracted from the geophone signal but uncertainties still exist as confirmed by flume experiments (Nicollier et al., 2021; Wyss et al., 2016a). Also, differences in bedload transport during snow and glacier-melt periods have been identified by means of monitoring stations equipped with geophone plates (Rickenmann, 2018) but the role of climatic factors in controlling bedload yield at different temporal scales has been poorly investigated so far.

In glacier-fed mountain basins, climatic factors exert a major control on the temporal and spatial evolution of sediment transfer. Climate change is increasing the sediment delivery from rockwalls due to freeze-thaw cycles and remobilization of sediment from glacier forefields and rock glaciers (Etzelmüller & Frauenfelder, 2009; Kofler et al., 2021; Lane et al., 2017; Savi, Comiti, & Strecker, 2021). Deglaciation in particular is causing intense and widespread redistribution of sediment from basin headwaters to the channel network, affecting landscape stability, water quality, and hence human health and livelihoods (Carrivick & Tweed, 2021). The current climate change, characterized by increasing temperatures and intense rainfall events, poses an additional challenge in terms of management of extreme hydrological events and consequent morphological changes (Borga et al., 2014; Raymond Pralong et al., 2015; Rinaldi et al., 2015). Warming temperature conditions change the seasonal patterns of both water discharge and sediment transport. Increasing glacier/snow melt runoff due to longer ablation periods as well as a spatial expansion of permafrost thaw enlarges the contributing drainage area of mountain catchments (Comiti et al., 2019; Li et al., 2021). To the best of our knowledge, the effects of nivo-glacial regimes on effective discharge for bedload transport have not been explored yet using actual transport data. The number of glacier-fed rivers monitored for bedload transport is rather limited and includes channels in Italy (Comiti et al., 2019; Mao et al., 2017), Switzerland (Delaney et al., 2018; Nicollier et al., 2021; Perolo et al., 2019; Schneider et al., 2016), Austria (Baewert & Morche, 2014; Habersack et al., 2017; Rickenmann, 2018), and Norway (Beylich & Laute, 2015; Bogen et al., 2015; Kociuba, 2017). See Mao et al. (2019) for a review of sediment transport monitoring in proglacial streams.

In this paper, we analyze a 7-year data set collected in the glacier-fed Sulden/Solda River (Italian Alps). Bedload fluxes in the study river are estimated by a novel approach based on the signal power to analyze the seismic data set detected by geophone plates. The high-frequency seismic data set allowed us also to explore which parameters of the recorded signals are best suited to predict bedload flux under both ordinary and intense transport rates. After presenting the developed methodology for the extraction of information on bedload transport from geophone-plate data, the paper will address the following objectives: (a) to analyze the temporal variability of bedload fluxes at different time scales (i.e., during single flood events as well as over different years), (b) to understand the role of climatic and geomorphic controls on bedload flux, and (c) to determine the contribution of different water discharges (and related runoff origin) in terms of cumulative bedload transport over the monitored period.

2. Materials and Methods

2.1. Study Area

The study area is the Sulden/Solda river basin, located in the upper Vinschgau/Venosta Valley (eastern Italian Alps), which is part of the Adige river basin (Figure 1a). The Sulden basin drains about 130 km^2 at the monitoring

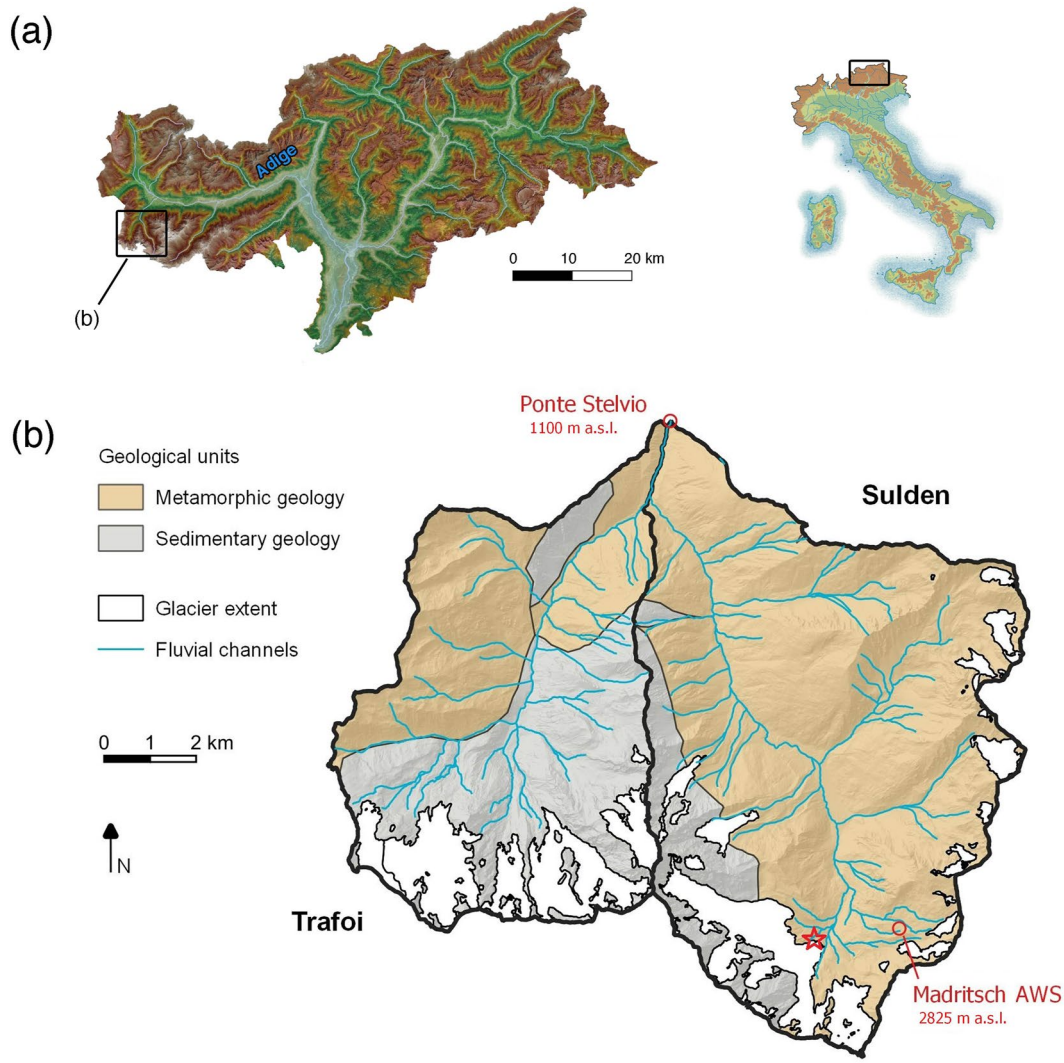

Figure 1. (a) Location of the Sulden/Solda and Trafoi catchments in the Vinschgau/Venosta Valley, Province of Bozen-Bolzano, Italy; (b) simplified geomorphic map of Sulden basin at the outlet defined by the village of Stilfserbrücke/Ponte Stelvio, where the monitoring station is located. The red star indicates the Sulden glacier front (see pictures in Figure 14).

station located at Stilfserbrücke/Ponte Stelvio, Autonomous Province of Bozen/Bolzano. The basin can be subdivided into the actual Sulden and the Trafoi sub-catchments that extend over 75 and 51 km^2, respectively (i.e., there are about 5 km^2, which drain below the Sulden-Trafoi confluence, Engel, Penna, et al., 2019; Buter et al., 2020).

The whole Sulden basin (Figure 1b) is characterized by a high topographic relief, ranging from around 1,100 m a.s.l. at the outlet of the basin to 3,905 m a.s.l. at the Ortler/Ortles peak, the highest mountain of South Tyrol. In 2016, the area covered by glaciers in the Sulden basin was around 18 km^2 (Autonomous Province of Bozen/Bolzano, 2017), representing 14% of the total basin area. The presence of glaciers (both debris-covered and clean ice), proglacial landforms, and extensive talus cover, combined with the high energy relief of the basin, results into complex and fast-evolving dynamics of sediment transfer (Buter et al., 2020). The upper basin hosts an automatic weather station (AWS) located at an altitude of 2,825 m a.s.l. (Madritsch/Madriccio station, run by the Meteorological Office of the Autonomous Province of Bozen/Bolzano). The Madritsch AWS records solar radiation, snow depth, and air temperature at 10-min intervals and precipitation at 5-min intervals.

The bedrock geology of the Sulden basin includes metamorphic rocks of the Ötztal- and the Campo-Crystalline (mainly composed by quartz phyllites, mica schists, and ortho- and paragneiss) and Permo-Triassic sedimentary carbonate rocks (Buter et al., 2020). Metamorphic rocks crop out in the eastern slopes of the Sulden catchment,

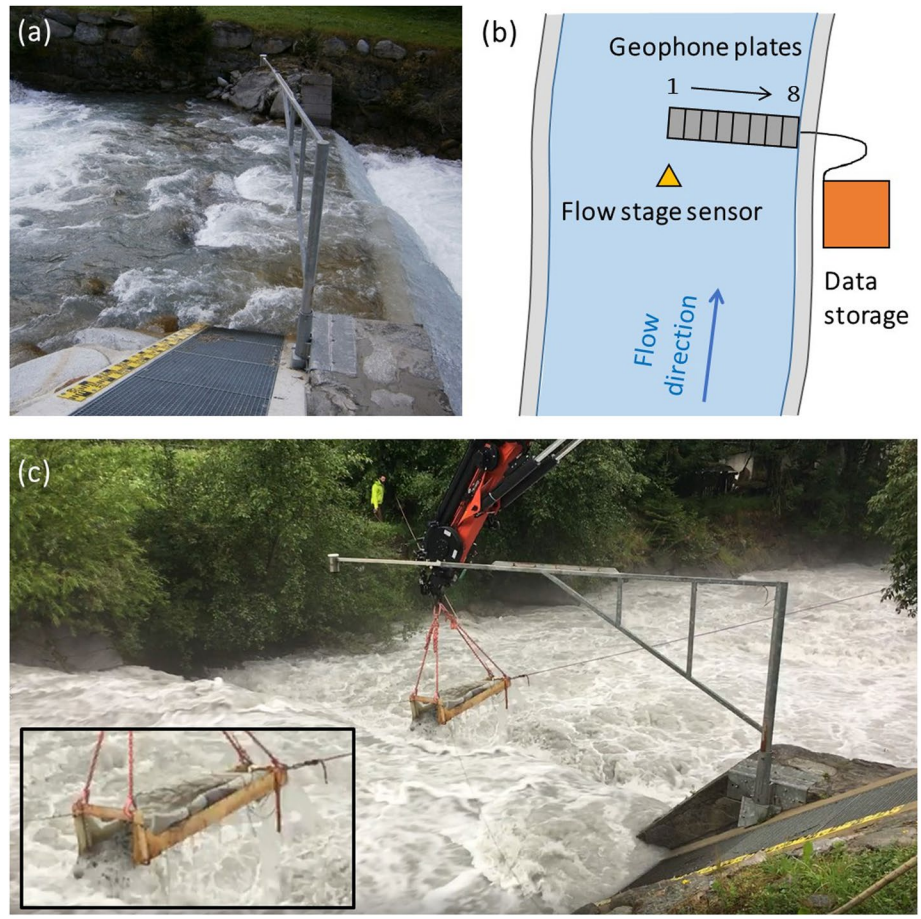

Figure 2. The Stilfserbrücke/Ponte Stelvio monitoring station on the Sulden-Solda River: (a) the check dam instrumented with the rack of geophone plates (red frame); (b) sketch of the monitoring station; (c) direct measurement with the portable trap (7 August 2019).

where they belong to the Permian orthogneisses of the Lasa unit, and western slopes of the Trafoi sub-catchement. Limestones and dolomites dominate in the Trafoi sub-catchment, but are also exposed on the western side of the Sulden sub-catchment, at a high elevation on the Ortler massif (Figure 1b).

The Sulden River has a nivo-glacial regime with the lowest runoff in winter and the highest runoff in summer. The flow recurrence intervals at the Stilfserbrücke station were estimated based on the annual maximum discharge values measured from 2014 to 2021. Adopting the Gumbel distribution, $Q_{1.5}$ and the Q_{10} are about 40 and 73 m^3/s, respectively. At the Stilfserbrücke station, the median and the 90th percentile of surface sediment grainsize distribution are 0.11 and 0.84 m, respectively, based on a grid-by-number sampling performed in the reach just upstream of the monitoring station, whose mean channel slope is 4.7%. The average slope of the entire Sulden channel from the glacier snout to the monitoring station is instead 8%. Snowmelt runoff dominates in May and June, whereas the glacier-melt period typically spans from July to late August–early September (Engel, Penna, et al., 2019). For the climatic period 1981–2010, mean annual air temperature (MAAT) at Madritch AWS was −2.4°C, whereas mean annual precipitation (MAP) averaged 980 mm (Savi, Comiti, & Strecker, 2021; 3PClim database).

2.2. Continuous Water and Bedload Monitoring

The monitoring station of Stilfserbrücke/Ponte Stelvio was designed to monitor both water and sediment fluxes (Figure 2). The construction and management of this station were the result of the cooperation between public institutions (Universities and local agencies) and private companies (Vignoli et al., 2016). At the station, suspended sediment transport is also measured by means of a turbidimeter (Engel, Penna, et al., 2019). In this work, we focus on bedload transport only, which is indirectly monitored by a set of eight geophone plates,

Table 1
Summary of the Geophone-Plate Data Set (2014–2020) Analyzed in This Paper: Number of Days of Complete Recording Available per Plate and Time Windows of Data Gaps in the Reference Period (Between Brackets)

	1 May–31 October 2014	14 May–30 October 2015	4 June–31 October 2016	30 May–27 September 2017	2 May–31 October 2018	21 May–28 October 2019	15 May–10 October 2020
Plate 1	184	170	122 (13 June–11 July)	121	163 (12–31 July)	110 (18 June–31 July)	147
Plate 2	160 (7–30 June)	170	122 (13 June–11 July)	121	177 (13–18 July)	110 (18 June to 31 July)	147
Plate 3	165 (12–30 June)	170	122 (13 June–11 July)	121	177 (13–18 July)	110 (18 June–31 July)	147
Plate 4	184	170	122 (13 June to 11 July)	121	177 (13–18 July)	110 (18 June–31 July)	147
Plate 5	184	170	122 (13 June–11 July)	121	177 (13–18 July)	110 (18 June–31 July)	147
Plate 6	184	170	122 (13 June to 11 July)	121	146 (13–18 July, 1–31 October)	110 (18 June–31 July)	147
Plate 7	154 (1–30 June)	170	122 (13 June–11 July)	121	155 (13–18 July, 3–24 September)	110 (18 June–31 July)	147
Plate 8	0	170	122 (13 June–11 July)	121	177 (13–18 July)	63 (18 June–31 July, 12 September on)	0

installed on the downstream end of a consolidation check dam (Figure 2a). The geophone plates cover 4 m corresponding to half of the river width (8 m) from the mid-channel to the right bank (Figure 2b), and are fixed on a concrete structure with a steel cantilever. Water level is measured at 10-min intervals and water discharge is calculated using a flow-rating curve calibrated by means of 27 direct discharge measurements, ranging from 1 to 20 m^3/s and performed in 2014 and 2015 using the salt dilution method.

The geophones are mounted on the underside of a 0.358-m long, 0.494-m wide, and 0.01-m thick steel plate. During bedload transport, gravel particles slide, roll or saltate over the steel plate. The geophone contains a magnet in a coil that acts as an inductive element. The plate transmits to the geophone sensor the vibration generated by bedload transport, and thereby, an electrical current proportional to the velocity of vibration is produced by electromagnetic induction inside the geophone. When the voltage exceeds a preselected very low amplitude threshold, A_{min}, the raw seismic signal sampled at 5 kHz is recorded.

Data recording started on 29 April 2014 and stopped on 6 November 2020. Some gaps affect the time series, especially in 2016, 2018, and 2019 due to technical problems (Table 1). In this paper, we analyze the period May–October (6 months per year), during which most bedload transport occurs.

2.3. Direct Bedload Measurements

Direct bedload measurements were performed using a portable bedload trap made by a net with an opening size of 3.6 mm, anchored to a metal frame and handled by a crane (Figure 2c). The sampling duration varied from 1 to 10 min, depending on the bedload transport intensity. During each measurement, the trap was inserted into the stream flow right downstream of a plate and held by a crane and four ropes, which helped to keep the trap stable at the sampling position. The sampling position was variable over the eight geophone plates (Table 2). We sieved the collected material (i.e., sediment particles larger than 3.6 mm in diameter, d) on site using four sieves with the opening size of 64, 45, 32, and 22 mm. The four separated sample classes ($d > 64$ mm, $64 > d > 45$ mm, $45 > d > 32$ mm, $32 > d > 22$ mm) and the finest fraction ($d < 22$ mm) were weighed and then released back into the stream. Particles with $d < 22$ mm were not sieved as controlled tests suggested that the geophone plates employed at Sulden (i.e., 1-cm thick) are unreliable—due to the sensitivity limit of the steel plates—for sediment size <1–2 cm. This latter range of sediment size is consistent with the lower detection limit identified in other sites, where 1.5-cm thick plates are employed (Rickenmann et al., 2012). We developed power function scaling relations between bedload directly measured with traps and the recorded seismic information:

$$Q_{b\,trap} = ax^b \quad (1)$$

where x represents a metric of the seismic signal (see Section 2.4) and Q_{btrap} the bedload rate at the reference plate (kg min^{-1}). In Table 2, the list of direct bedload measurements is reported. The minimum and the maximum measured values of $Q_{b\,trap}$ are 0.27 kg min^{-1} (25 June 2020) and 54.35 kg min^{-1} (7 August 2019).

Table 2
List of Direct Bedload Measurements Performed by the Portable Trap From 2014 to 2020: Number of Measurements (Used for Calibration After Data Validation), Total Bedload Mass ($d > 3.6$ mm) Extracted, Reference Plate of the Direct Measurements (Plate Number), d_{50} (Daily Mean Value), and Water Flow Conditions (Daily Range) During Measurements

	Number of measurements	Sampled bedload mass (kg)	Reference plate	d_{50} (mm)	Water discharge ($m^3\ s^{-1}$)
5 June 2014	3 (2)	22.8	5, 6	11.3	7.7–7.8
6 August 2014	5 (4)	84.2	3, 4, 5, 6	19.7	19.7–20.1
9 September 2014	3 (2)	32.2	7	13	6.5–6.7
22 July 2015	6 (5)	353.6	5, 7	22	19.6–20.3
13 August 2015	9 (9)	395.6	1, 5, 6, 7	18.2	13.6–13.9
7 September 2017	9 (8)	100.5	1	n.a.	7.2–7.4
23 August 2018	5 (4)	182.3	1	14.2	14.3–14.5
7 August 2019	9 (9)	347.95	1, 2, 3, 4	14	21.1–21.2
25 June 2020	8 (6)	121.5	1, 3, 4, 5	10	12.8–14.1
22 July 2020	10 (8)	217.75	2	12.6	12.8–13.2
27 August 2020	8 (8)	208.2	1	16	9.2–11.8

Note. Grain size data of the bedload measurements performed in 2017 are not available (n.a.).

2.4. Processing of Geophone-Plate Data

Data gathered at the geophone plates are sampled at 5 kHz and recorded continuously. A detection algorithm based on an intensity-duration (I-D) threshold together with a Portable Network Graphics (PNG) compression allows the recording of the raw signal. A very low I-D threshold activates the recording of the signal, while below that threshold zero values are saved (i.e., no transport). The raw signal is then compressed in PNG files that contain about 7 min of signal each and occupy from few hundreds of KB to few MB, see supplementary material for details. The saved data can be analyzed by counting the number of impulses above a given threshold (i.e., the "traditional" geophone-plate signal elaboration described by Rickenmann et al., 2014) and by applying any type of signal processing. We extracted three basic signal metrics from the raw signal, calculated over a 1-min time window: the maximum amplitude A_{max}, the number of impulses Imp, and the signal power P (Figure 3).

The transformation of a raw signal into a rate of impulses per unit of time consists of counting how many times the signal exceeds a threshold after crossing the horizontal axis in a given time period (Figure 3a). Assuming a constant flow velocity, the energy transfer from the flow to the plates is controlled by the sediment concentration, the grain size, and the flow turbulence (Coviello et al., 2018; Gimbert et al., 2014; Turowski et al., 2015). We tested four different exceedance thresholds (0.01, 0.04, 0.16, and 0.32 V) for the transformation of the raw signal into impulses, similar to what has been proposed for the analysis of the Japanese pipe (Mao et al., 2014; Mizuyama et al., 2003). The number of impulses recorded in a given time period is threshold-dependent. The need to select the threshold value represents a possible drawback of such an approach because (a) it is site-dependent and (b) it should be adapted to transport conditions. These limitations have been already observed in the field of debris flow seismic monitoring, where the transformation into impulses has been also employed in the past (Arattano et al., 2014). The values of A_{max} are computed as the maximum voltage amplitude (V) reached by the raw signal during the 1-min sampling interval (Figure 3a). The signal power P (Figure 3b) is calculated as the integral of the squared amplitudes over a 1-min time window by using the following formula, where $T = 1\text{min}$:

$$P = \frac{1}{T}\int_{t_1}^{t_2} |u(t)|^2 \mathrm{d}t \tag{2}$$

2.5. Effective Discharge

The availability of a multiannual data set of both water discharge and bedload rates at the minute-scale resolution allows the quantitative investigation of discharges that over long-term time periods transport most of the

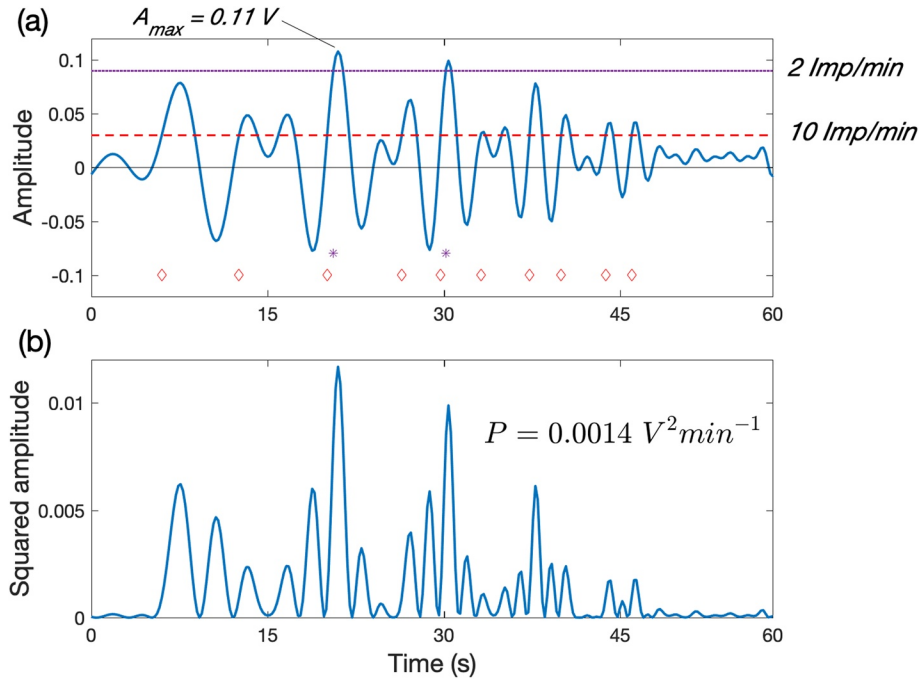

Figure 3. Extraction of the main signal metrics from a seismic signal. (a) Time series of a synthetic signal voltage output (blue line), maximum voltage amplitude (A_{max}), and impulses per 1 minute that exceed two different thresholds (i.e., violet- and red-dashed lines). Violet stars and red diamonds represent the impulses counted for the two different thresholds. The impulse rates resulting from the two thresholds are indicated on the secondary *y* axis. (b) Signal power (P) calculated summing the squared amplitude values over a time window of 1 min (see Equation 2).

sediments, that is, the flows that are most effective for bedload transport (Wolman & Miller, 1960). Such effective discharge is a function of both the intensity and the frequency of occurrence of flow conditions transporting sediments. Building upon this concept, Lenzi et al. (2006) applied a data-driven method to calculate the effective discharge curve for bedload transport E_Q based on the average bedload rate measured—and not estimated by transport capacity equations or bedload rating curves, as most commonly done—for each flow class:

$$E_q = Q_b * f \tag{3}$$

where Q_b is the bedload rate (kg min^{-1}) and f is the flow frequency (%). The flow class associated with the maximum value of E_b indicates the effective discharge for bedload during the monitored period. In this work, we adopt this method to perform a magnitude-frequency analysis of bedload transport rates using flow class intervals of 4 m^3 s^{-1}. We calculated the effective discharge curve E_Q using the average transport rate for each flow class interval of the 7-year data set collected in the Sulden River. For each monitored year, one reference plate was selected based on two criteria that are (a) the completeness of the monitoring data set (see Table 1) and (b) the higher bedload rates measured along the cross section. Such magnitude-frequency analyses are utilized to investigate the impact of different runoff origins (rainfall events, snowmelt, and glacier-melt flows) on bedload transport.

3. Results

3.1. Direct Bedload Measurements

From 2014 to 2020, 76 direct bedload measurements were carried out, but only 65 of them were used for calibration after a validation of the data set. Data validation consisted in eliminating the samples affected by clear problems encountered during the measurements (e.g., unstable trap or positioned onto the geophone plates) or that represented outliers of the paired values of extracted mass versus the signal metrics described below (i.e., exceeding two standard deviations of the distribution). In total, about 2,068 kg of bedload were used to derive the calibration functions after this validation procedure (about 86% of the total sampled mass).

The three signal metrics used for calibration are (a) impulse rates, (b) the maximum amplitude, and (c) the signal power (Figure 4). We extracted the impulses per minutes using four different thresholds and divided the

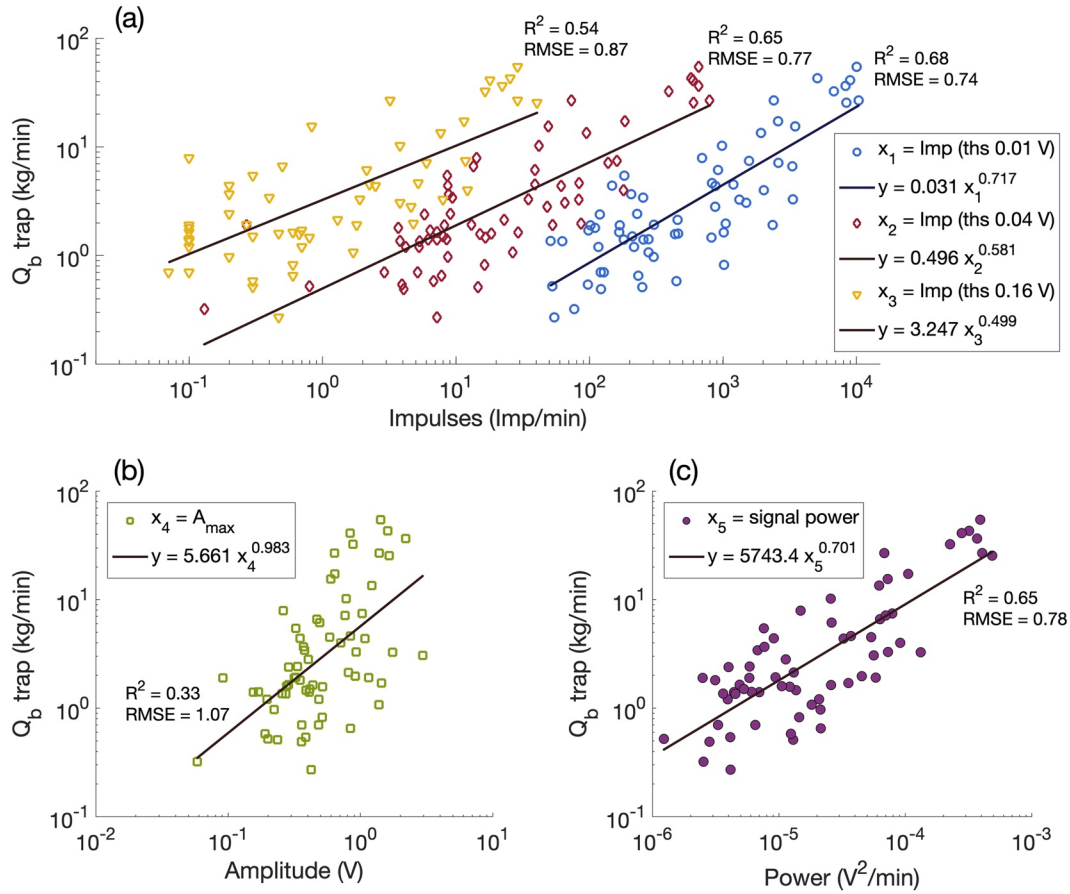

Figure 4. Geophone-plate calibration relationships of bedload rates as a function of (a) the impulse rate calculated with three different voltage thresholds, (b) the maximum voltage amplitude within a 1-min window, and (c) the signal power computed per minute. For each equation, the coefficient of determination (R^2) and the Root Mean Square Error are reported.

sampled weight and the number of impulses by the sampling duration to obtain the bedload rate (kg min^{-1}) and the impulse rate (Imp min^{-1}). Then, each pair of values was plotted (Figure 4a). A lower threshold (i.e., 0.01 V) leads to a higher number of impulses. Raising the threshold, the number of impulses decreases and progressively some data points disappear from the plot. For this reason, we selected three thresholds to be tested for calibration (0.01, 0.04, and 0.16 V). The relation of impulse rates to the largest threshold, 0.32 V, resulted in strong data scatter and is not shown here. The lowest threshold produced the largest number of impulses and yielded the highest correlation coefficient and the lowest error when a power law regression is applied (Figure 4a). The regressions of impulse rates with A_{max} and signal power P are reported in Figures 4b and Figure 4c, respectively. In Figure 4, the coefficients of determination and the prediction errors of the different regression equations are reported. The p-values of all equations are <0.001.

Figure 5 shows the—relatively small—coarsening of the bedload grain size distribution (GSD) with increasing flow discharge. The GSD of 57 measurements out of 65 is presented for three classes of discharge: 6.5–12 (low), 12–15 (medium), and 19–21 $m^3 s^{-1}$ (high). In general, largest discharges result in slightly coarser bedload material as a consistent pattern among the three discharge classes is visible. An exception is represented by sediments with $d < 22$ mm, for which the medium discharge class features the highest proportion. The difference between the cobble-boulder bed material (d_{50} about 40 mm) and the comparatively finer bedload (d_{50} about 15 mm) indicates that, for the 6.5–21 $m^3 s^{-1}$ discharge range, the stream transports its gravel bedload over an immobile bed.

3.2. Estimation of Bedload Yield

In Figure 6, we show the annual bedload yield ($d > 3.6$ mm) at Stilfserbrücke calculated using the three calibration equations described in Section 3.1, which are based on different signal metrics (impulses, maximum voltage,

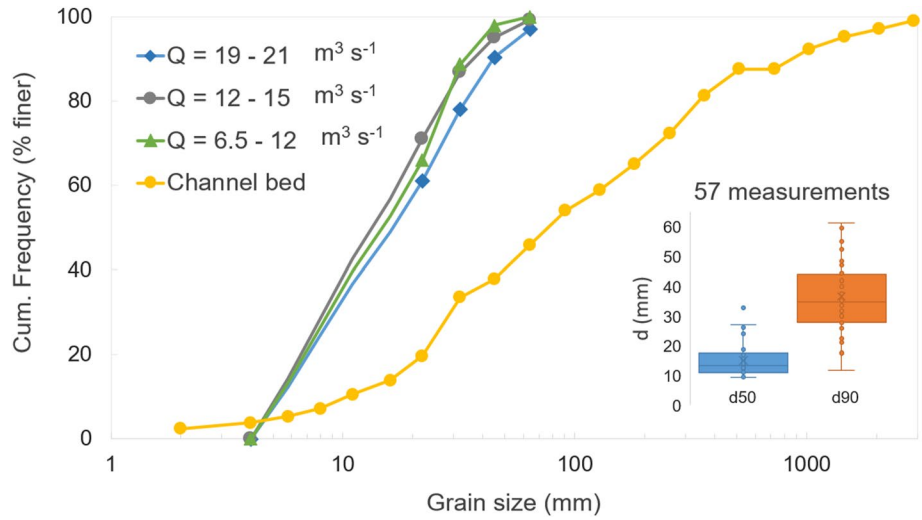

Figure 5. Grain size distributions (GSD) of bedload transport measurements taken by the portable trap and the channel bed material based on a grid-by-number sampling performed in the reach just upstream of the monitoring station. For better visibility of trends, the grain size distributions are presented for classes of discharge. In the inset, boxplots representing the distribution of d_{50} and d_{90} for the available GSD data set (57 bedload measurements out of 65).

and signal power). For impulses, we selected the calibration equation based on the impulses calculated with a threshold value of 0.01 V, given its highest correlation coefficients. Data gaps on single plates were filled using data collected on neighboring plates in order to deliver homogenous annual values (Figure 6). Linear interpolation was used to estimate the bedload mass in case of data gaps with a correcting factor of 0.7 going from center to right bank. The latter correcting factor was calculated based on the decrease of the signal intensity from plate 1 (mid channel) to plate 8 (right bank); see bar plots in Figure 6. For 3 years (2016, 2018, and 2019), it was not possible to fill some data gaps that occurred during the summer on all geophone plates (Table 1). Because only half of the monitored river cross section is equipped with geophone plates, the final bedload mass was obtained doubling the calculated values by assuming a symmetrical distribution of bedload transport across the section. Such an assumption is considered sufficiently valid due to the straight, engineered geometry of the Sulden channel upstream and downstream of the monitored section.

The calibration equation based on the maximum amplitude results in lower estimates of bedload transport, while the two other equations (impulses and signal power) return more comparable values. However, there are specific years (i.e., 2014, 2016, and 2020) where annual yields obtained from computations based on the signal power and the maximum amplitude differ notably (Figure 6). These latter years are characterized by intense bedload events and—similar to what has been observed for the maximum amplitude—it seems that the number of impulses is dampened or truncated at high bedload rates. More details on the computation of the bedload rate based on those two parameters are reported in the discussion section. Hereafter, the bedload rate at one single plate Q_{bn} (kg min^{-1}) is calculated by means of the signal power (P) equation:

$$Q_{\mathrm{bn}} = 5743.4P^{0.701} \tag{4}$$

and the bedload rate Q_b (kg min^{-1}) and bedload concentration C_b (kg m^{-3}) at the whole cross section (8-m long) are estimated as

$$Q_b = 16Q_{\mathrm{bn}} \tag{5}$$

$$C_b = \frac{Q_b}{Q} \tag{6}$$

given that one plate occupies $\frac{1}{16}$ of the channel width.

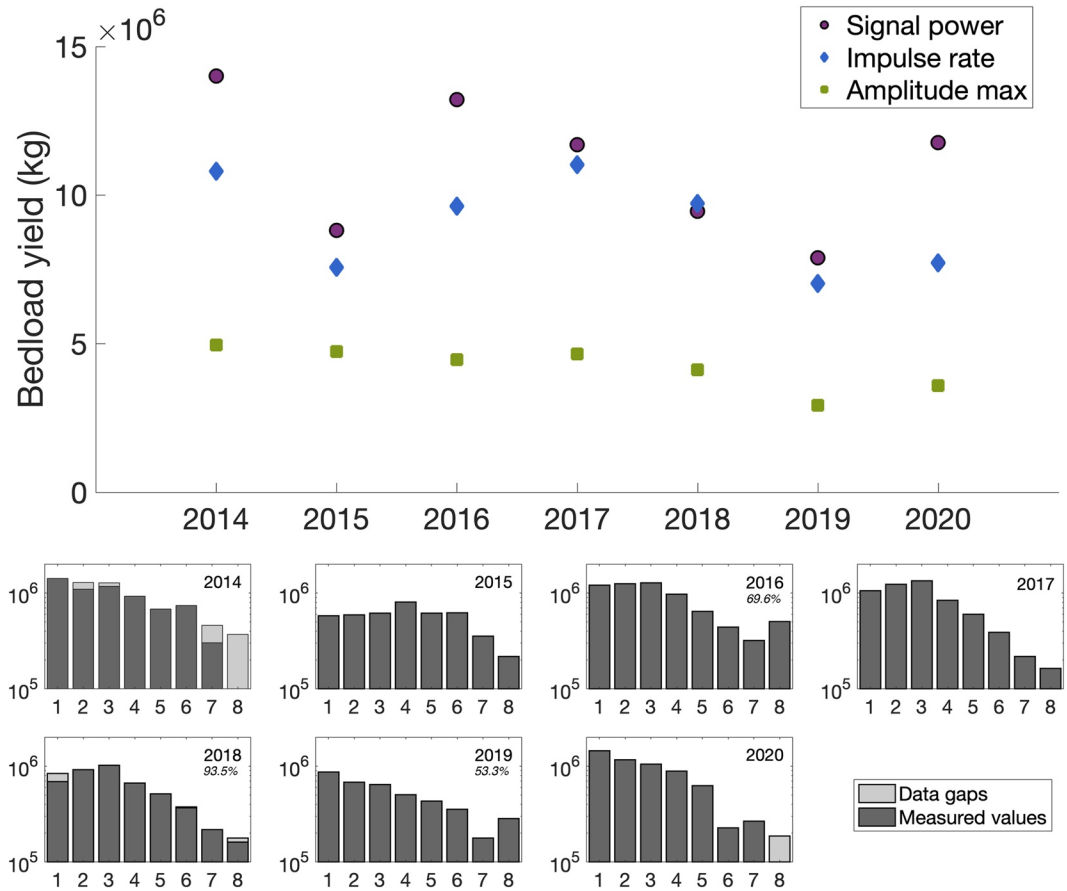

Figure 6. Annual bedload yield (kg) from 2014 to 2020 calculated using three calibration equations based on the signal power, impulses calculated with a threshold of 0.01 V, and the maximum amplitude. Some years are affected by important data gaps in June and July (28 days in 2016, 6 days in 2018, and 43 days in 2019). Bar plots report annual yields (kg) at each plates (1 = central plate, 8 = plate bordering the right bank) each year. Percentages indicate the completeness of the data set, when the value is not indicated it means 100%.

3.3. Continuous Bedload Transport Data and Hydrometeorological Variables

In Figure 7, the water discharge and unit bedload rate measured at the Stilfserbrücke station are shown for the whole monitoring period, along with hydrometeorological data (daily precipitation and mean air temperature) and snow cover measured at the Madritsch AWS.

In Figure 7, the unit bedload rate q_b is calculated using data collected at plate 1 only, near the channel center, applying Equation 4. The seasonal variability of hydrometeorological variables is well visible together with short-scale fluctuations due to intense rainfall events and snow-melt periods in late spring/early summer. Water discharge ranges from values of about 5 $m^3\ s^{-1}$ before to 30 $m^3\ s^{-1}$ during the snow- and glacier-melt periods. Peak values of flow discharge higher than 40 $m^3\ s^{-1}$ are reached at a few flood events. As expected, the most important peaks in water discharge and unit bedload rate occurred during the same events (e.g., 13 August 2014, 12 July 2016, and 29 August 2020); however, unit bedload rates show a remarkable variability of more than three orders of magnitude.

We performed a magnitude–frequency analysis to compute the discharge values that transported the largest amount of sediment over the analyzed period of 7 years. By using the Lenzi et al. (2006) approach (see Section 2.5), the average, 10th and 90th percentiles of bedload transport rate associated with each flow class were calculated (Figure 8a). The bedload rate Q_b at the cross-section scale was estimated by using Equation 5. Then, the value of E_q for each flow class was calculated multiplying the actual flow frequencies and mean bedload rates measured at the station (Figure 8b). Interestingly, the E_Q curve does not present a single relative maximum, but instead presents three relative peaks, respectively, at about 18, 42, and 70 $m^3\ s^{-1}$, corresponding to summer glacier-melt

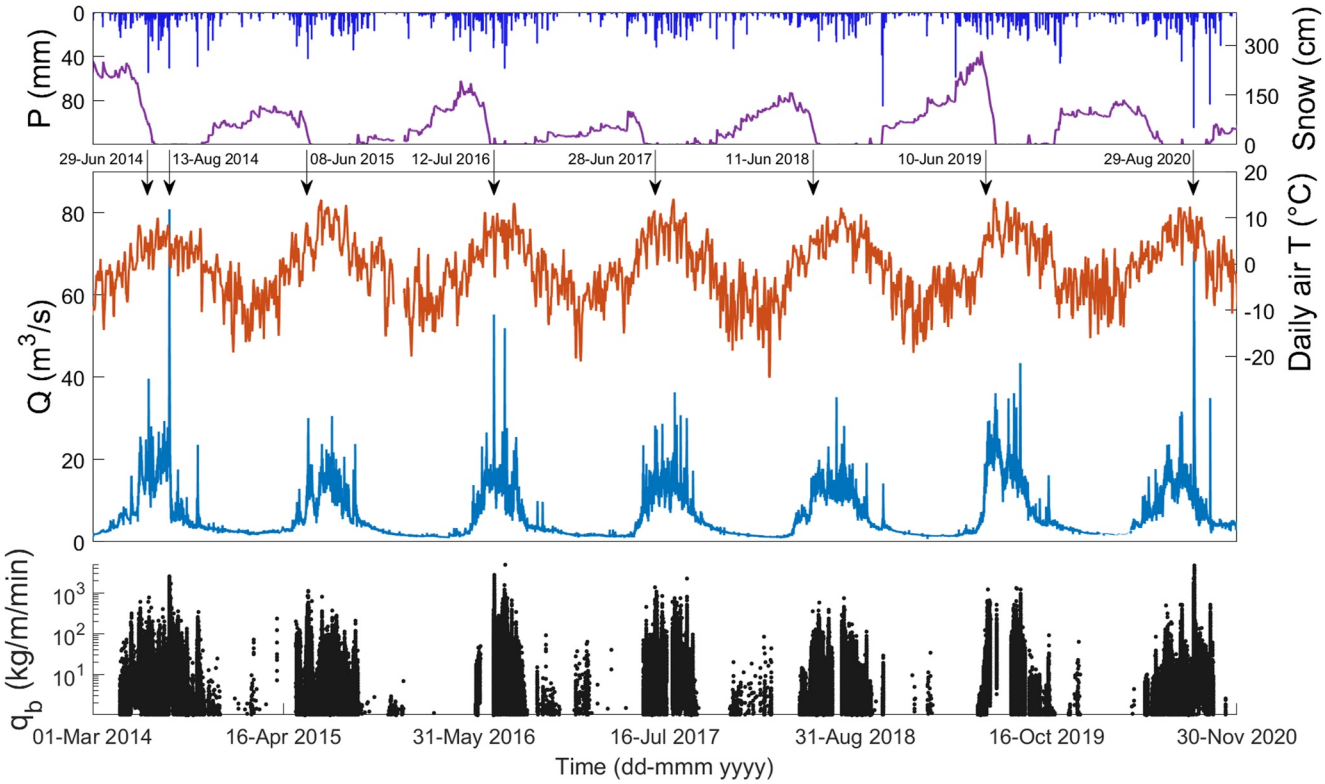

Figure 7. Hydrometeorological data from the Madritsch automatic weather station (precipitation, snow depth, and air temperature) and flow discharge and unit bedload rate (at plate 1) measured at Stilfserbrücke from 2014 to 2020. Some events investigated in detail in this work are marked with black arrows.

flows, 1.5–2 years flood flows, and to the highest discharges occurred in the monitored period, respectively. The physical interpretation of such a complex pattern for the E_Q curve—and of its peak values—will be presented in the discussion section.

3.4. Analysis of the Temporal Variability of Bedload Transport

The bedload rate was normalized by the associated flow discharge to investigate the impact of factors other than runoff (i.e., sediment supply) on bedload transport. To this aim, we present the variability of bedload concentration C_b through time (Figure 9).

The bedload rate Q_{bn} at the selected reference plate n was calculated using the power function that the related bedload rate to the signal power (Equation 4). The computed time series of bedload concentration C_b show a remarkable variability through time. The highest values of bedload concentration C_b are usually observed in June, July, and August (Figure 9) but the trend is irregular. In particular, 2014 and 2020 feature two bedload events that dominate the distribution. Other years, such as 2017 and 2018, do not present intense events but a moderate and regular bedload transport from early June to the end of August.

In Figure 10, we analyze the complex relation between Q_b and Q for a single year, 2014, for which the time series record is complete and captures an intense flood event ($>Q_{10}$). We used data gathered at plate 1 to draw the figure as they are representative of the maximum bedload rate observed at the cross section in 2014 (see bar plot in Figure 6). In Figure 10a, the temporal evolution of C_b from 1 May to 31 October 2014 is plotted together with the daily precipitation in the upper Sulden basin (data from Madritsch AWS). The maximum bedload concentration is reached on 13 August 2014, when a large flood event was triggered by a precipitation event that featured a cumulated rainfall of 50.9 mm in 24 hr. In the scatterplot (Figure 10b), the measured values of bedload rate are aggregated at 10-min time intervals (i.e., the recording frequency of the flow stage sensor) and grouped into three time periods: May–June, July–August, and September–October. The first time period (Figure 10c, late spring/early summer) features a generally positive trend of bedload transport rates with discharge, although data scatter

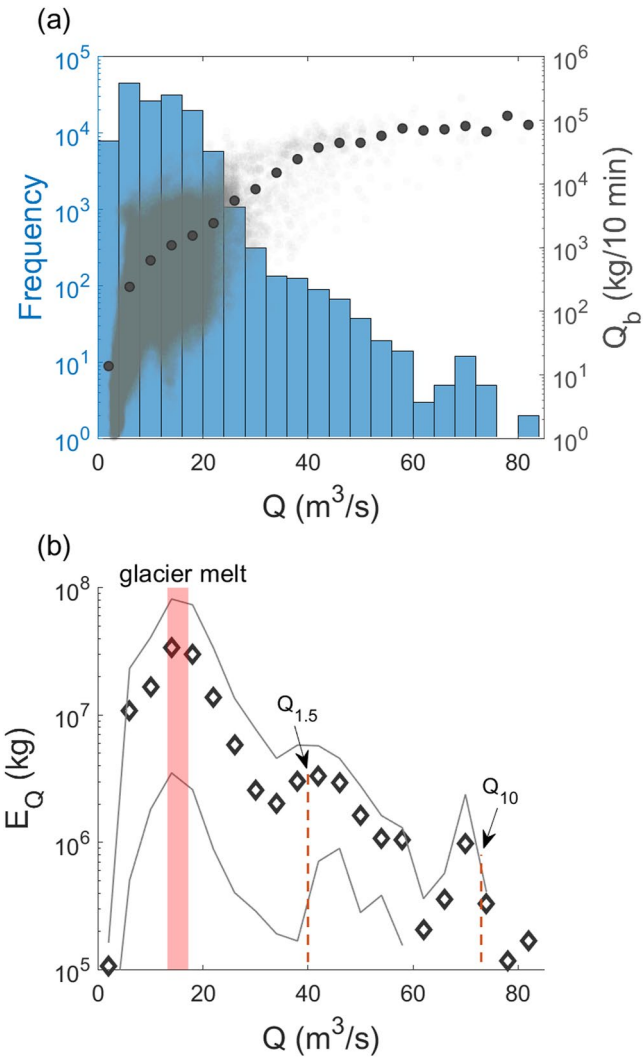

Figure 8. Combined plot (a) of the absolute flow frequencies (number of occurrences) and associated bedload rates at the Stilfserbrücke station for the 2014–2020 period. In (a), the shaded area and the larger dots represent the entire data set of bedload rates and the mean value for each class, respectively. In (b), the resulting product of the two variables is shown; the continuous gray lines are calculated using the 10th and the 90th percentiles of the bedload rate distribution.

over two orders of magnitude. The second time period (Figure 10d, warmer summer weeks) is characterized by the largest bedload variability of four orders of magnitudes, and the third time period (Figure 10e, late summer) shows a general decrease of bedload transport with discharge. A similar seasonal trend is observed for most of the following years (see Figures S5–S10 in Supporting Information S1), except for 2015 during which the highest bedload rates were observed in May–June due to the combination of rainfall and snowmelt (Figure 11c), and probably, to the memory effect of the 2014 flood.

Figure 10a shows how very similar values of cumulated rainfall in 24 hr in the upper basin (29 June, 13 August, and 13 October) are associated with very different responses in terms of bedload export.

Figure 11 provides the analysis of bedload rates versus discharge at the event time scale, combined with the information on the precipitation, temperature, and snow cover conditions in the upper basin. For eight bedload event that occurred from 2014 to 2020, in Figure 11, we report the mean air temperature Ta_{3d} at the Madritsch AWS as well as the variation of snow height in the analyzed time windows of 3 days. Table 3 shows for these events the unit bedload peak rate estimated at the reference plate, along with the peak discharge and the main runoff origin during each event. The flood event that occurred on 13 August 2014 transported about 4,500 tons of bedload in 96 hr (30% of the annual transport), featuring a bedload peak of 10^4 kg m^{-1} min^{-1}. In mid-August, there was no snow cover in the upper basin. On August 13, the mean air temperature calculated on the previous 7 days Ta_w was 7.1°C and the mean air temperature calculated on the previous 3 days Ta_{3d} was 7.8°C (Figure 11b). In the following 3 days, the bedload rate remained quite intense, ranging from 10^2 to 10^3 kg in 10 min, while flow discharge decreased from 80 m^3/s to about 10 m^3/s, inducing a counterclockwise hysteresis cycle (Figure 10d). A very similar precipitation event that occurred on 29 June 2014 (54.9 mm in 24 hr) produced a bedload event with a peak value of 10^3 kg m^{-1} min^{-1} (Table 3), one order of magnitude lower than the one occurred on 13 August 2014. Indeed, the precipitation event of 29 June 2014 did not result in a significant response in terms of bedload transport because it occurred under very different weather conditions ($Ta_w = 3.9$ °C and snow cover in the upper basin) that likely impeded particle motion in the headwaters.

This complex interaction between hydrological and climatic parameters is confirmed by the analyses of the main bedload events that occurred in the following years. Bedload events occurring in June (Figures 11a, 11c, 11e, 11f and 11g) generally feature lower bedload peaks than events occurring from mid-July to August. Major bedload events, like the ones that occurred on 13 August 2014 and 29 August 2020, were triggered by large precipitation events (more than 50 mm of cumulated rainfall in 24 hr) occurring after warm summer days, and when the upper portion of the basin was mostly free from snow cover. On 29 August 2020 (Figure 11h), 8,100 tons of bedload were transported in 72 hr, which correspond to the 70% of the annual transport. Hysteresis cycles (counterclockwise) are clearly visible only for the events occurred on 13 August 2014 and 12 July 2016 (Figures 11b and 11d).

4. Discussion

4.1. Advantages of Using a Calibration Equation Based on the Signal Power

Analysis of the geophone plates data showed how the bedload estimation performed with different signal metrics can differ significantly. The calibration based on the maximum amplitude underestimates the annual bedload yield of about 50% compared to impulse rates. The explanation for this underestimation is that the raw signal sampled at 5 kHz exceeds the full scale (i.e., 10 V) during periods of intense transport. Consequently, the

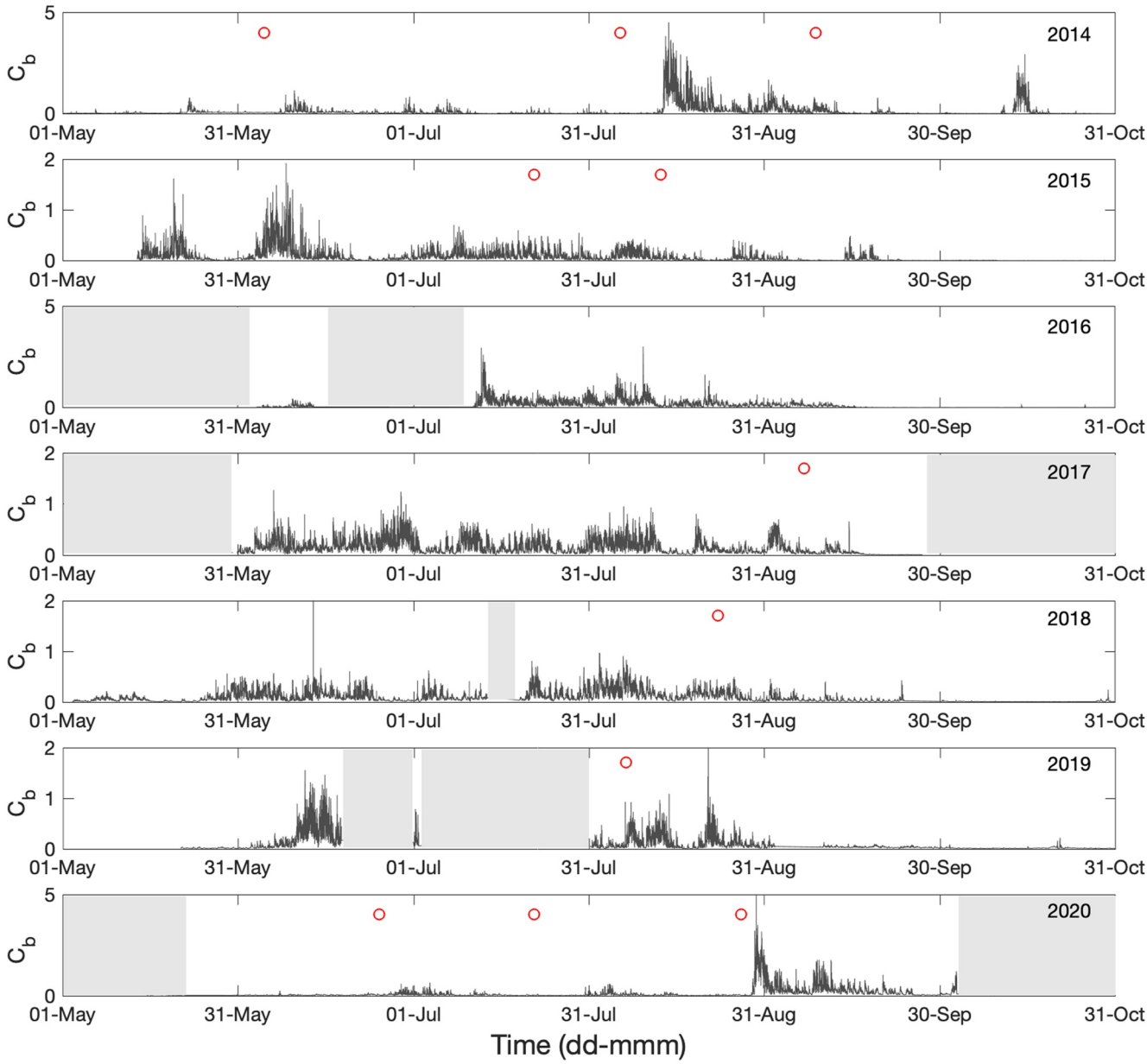

Figure 9. Bedload concentration (kg m^{-3}) measured from 2014 to 2020 at the Stilfserbrücke station. C_b is calculated using data from plate 1 in 2014, 2019, and 2020; plate 4 in 2015; and plate 3 in 2016, 2017, and 2018. Gray areas represent data gaps in the seismic recordings. Red circles indicate days during which direct measurements were performed (see Table 2 for details). Note that the upper *y*-axis limit is not constant (it is 5 for 2014, 2016, and 2020; 2 for the other years).

maximum amplitude is not representative of high bedload rates. This clipping of a single short-duration peak (i.e., the highest value in the analyzed 1-min window) would produce a marked reduction of the maximum amplitude. Moreover, the maximum amplitude cannot differentiate between the case of one or more than one similar impacts in each time interval of 1 minute, a condition that is very likely met during high bedload transport. In contrast, the signal power would be significantly less affected as it is calculated as the integral of the squared amplitude over the 1-min time window. Computation based on the impulse rate strongly depends on the chosen threshold despite the three calibration curves showing similar fit statistics. This effect is well-visible comparing the bedload rate time series calculated with the signal power and different impulse equations (Figure 12). July 2016 is a month of intense bedload transport due to two flood events that occurred on 12–15 and 29–31 July (Figure 12a). Adopting the impulse equation with threshold 0.01 V, the bedload peak of this latter event is damped by one order of magnitude (Figure 12b), producing an underestimation of bedload volume of more than 50% for the whole

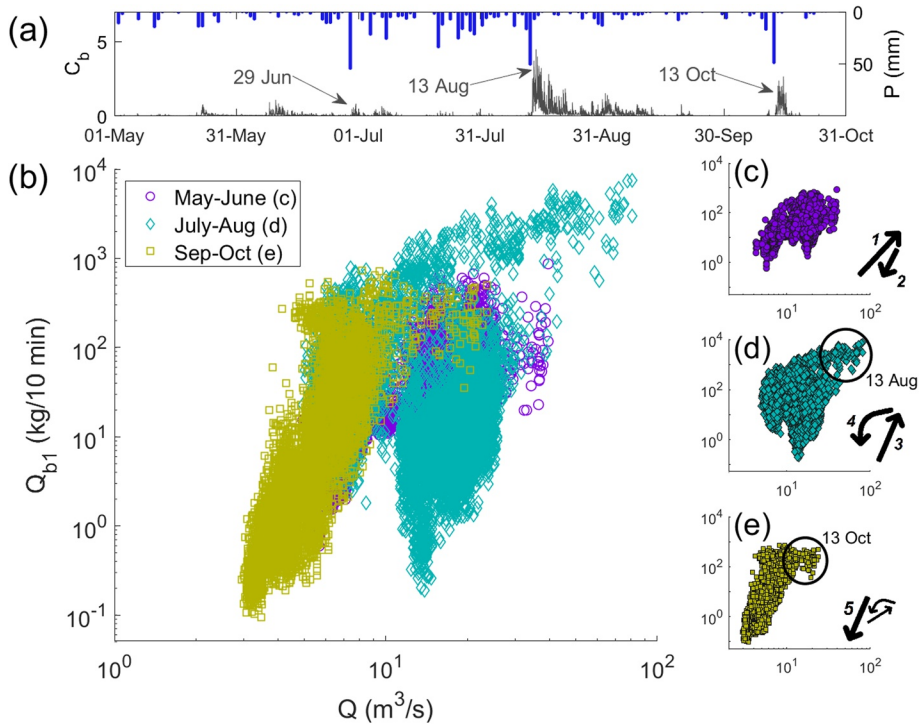

Figure 10. (a) Bedload concentration measured at the Stilfserbrücke station (plate 1) and daily precipitation at Madritsch AWS from 1 May to 31 October 2014. (b) Scatterplot of bedload rate measured at plate 1 versus discharge. Data are separated in three insets following the bimonthly classification: (c) May–June, (d) July–August, and (e) September–October. In the insets, the black arrows indicate how points move over time and show the seasonal hysteresis cycles (clockwise in May–June, counterclockwise in July–August). On 13 October, a bedload event produces a short-term counterclockwise hysteresis.

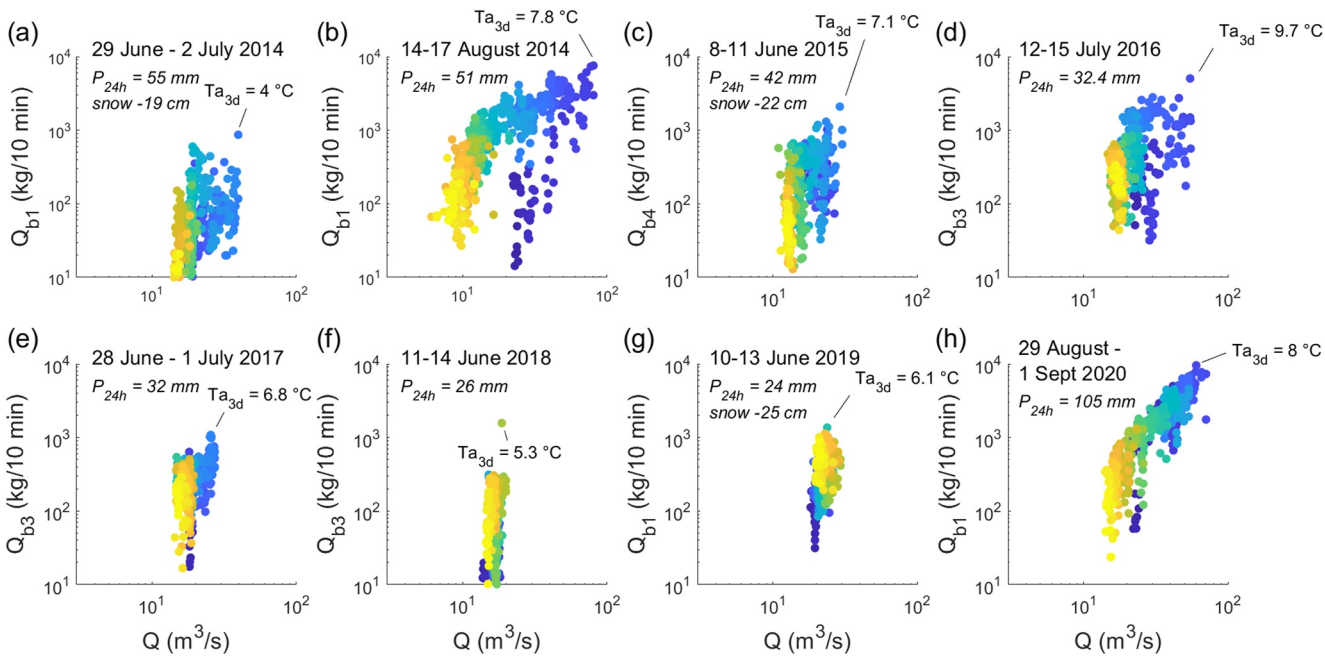

Figure 11. Bedload rate measured at plate 1 versus discharge of the main flow events occurred from 2014 to 2020. Reported bedload rates are measured at one reference plate (plate 4 in 2015, plate 3 in 2016–2018, and plate 1 in 2019–2020). The variation of snow height refers to the investigated period of time and when it is not indicated means absence of snow cover. Snow cover and mean air temperature are calculated using data gathered at the Madritsch automatic weather station. The rainbow color scale (from blue to yellow) follows the time line.

Table 3
List of the Main Bedload Events Occurred From 2014 to 2020 at Sulden

Date	Event duration (hours)	Peak discharge (m^3 s^{-1})	Unit bedload peak rate (kg m^{-1} min^{-1})	Runoff origin
29 June 2014	72	39.6	$1.7 \cdot 10^3$	Snowmelt and rainfall
13 August 2014	96	80.8	$1.51 \cdot 10^4$	Glacier melt and rainfall
8 June 2015	72	30.1	$4.1 \cdot 10^3$	Snowmelt and rainfall
12 July 2016	72	55.2	$1.01 \cdot 10^4$	Glacier melt and rainfall
28 June 2017	72	27.2	$2.1 \cdot 10^3$	Glacier melt and rainfall
11 June 2018	72	20	$3.1 \cdot 10^3$	Glacier melt and rainfall
10 June 2019	72	29.3	$2.7 \cdot 10^3$	Snowmelt and rainfall
29 August 2020	72	70.5	$2.83 \cdot 10^4$	Glacier melt and rainfall

Note. For each event, starting date, duration, peak discharge, unit bedload peak rate based on the reference plate, and main runoff origin are reported.

month. The dampening of the impulse curve does not occur during low-intensity transport periods (e.g., 16–20 July) when the signal fluctuates well below the clipping threshold (the dashed line). Adopting impulse equations calculated with higher thresholds (0.04 V in Figure 12c and 0.16 V in Figure 12d), the clipping threshold progressively rises and the underestimation of the monthly bedload yield reduces. However, such higher thresholds are less sensitive to low-amplitude signals commonly generated during finer, lower-intensity bedload events and thus may also lead to an underestimate of total bedload volumes. As a result, compared to the signal power, impulse rates underestimate the annual bedload yield by up to 20% and the peak bedload rate by more than one order of magnitude (Figure 6 and Figure S4 in Supporting Information S1). In fact, an overly low-impulse threshold leads to the underestimation of bedload peak rate, which significantly contributes to the annual bedload yield during periods of intense transport.

This bedload underestimation is the result of the well-known phenomenon of impulses saturation (Arattano et al., 2014), that is, for high amplitude signal oscillations, the number of impulses does not increase anymore once the clipping value is reached. The computation of signal power requires the raw signal to be saved and post-processed, but in most geophone-plate measuring station, the raw signal is not stored and the impulse rates are calculated in real time in order to save disk storage space. In previous studies based on data from multiple streams, it was argued that the similarity between the regression coefficients of impulses and signal power equations indicate that impulse rates are suitable to predict the transported bedload mass (Rickenmann et al., 2014). In the Sulden River, we obtained very similar regression coefficients for the two equations (i.e., $R^2 = 0.68$ for impulses and $R^2 = 0.65$ for the signal power). However, regression coefficients alone do not explain completely the process dynamics. In the field of debris-flow seismic detection, it is well-known that selecting a threshold that is too low can impede the correct representation of the different debris-flow surges, and on the other hand, choosing a higher threshold can result in the signal damping (Arattano et al., 2014). Here, we showed that the power of the geophone-plate signal better represents the variability of bedload transport than impulses, incorporating the advantage of both low and high thresholds to compute the impulse rate.

We also explored possible relationships between the signal power and the bedload GSD. There is a positive correlation between the d_{90} of the direct bedload measurements and the signal power, while the d_{50} does not show any significant correlation (see Figure S3 in Supporting Information S1). Vibrations produced by larger cobbles feature higher intensities and can dominate the energy deliver to the channel bed (Turowski et al., 2015; Wyss et al., 2016a). Recent controlled flume experiments show how the increasing flow velocity reduces the signal response in terms of number of packets/impulses and the GSD variability of the transported bedload can influence the signal response of geophone plates (Nicollier et al., 2021). In addition, the signal response is influenced by the structure of the monitoring station, that is, number of plates and dimensions of both the steel frame and impact plates.

4.2. Factors Controlling Bedload Rates and Yields

The analysis of continuous bedload data collected in the Sulden River highlights the complex interaction between hydrometeorological parameters in controlling bedload variability. In steep mountain rivers, bedload transport

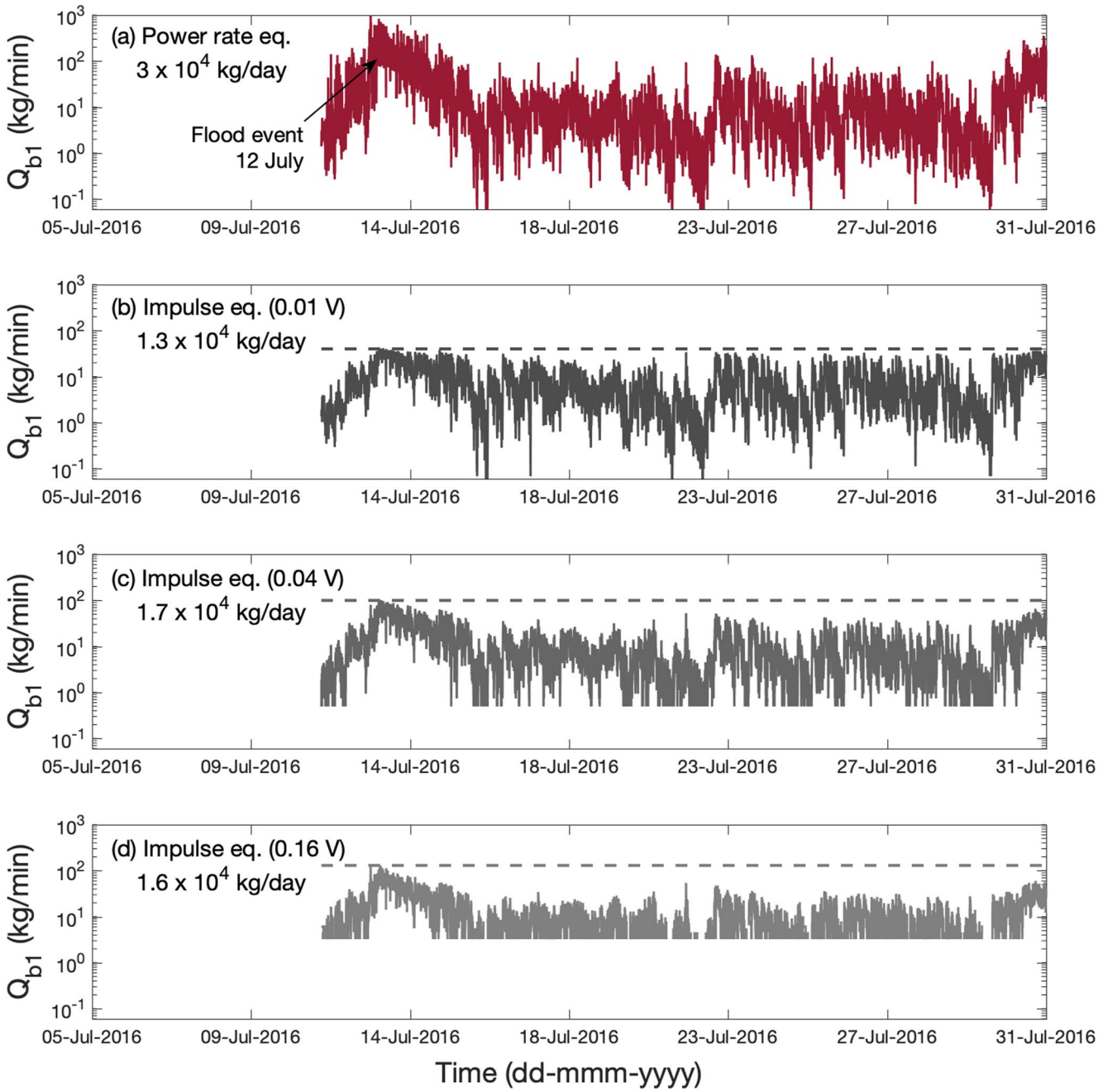

Figure 12. Bedload rate (kg/min) at the plate 1 calculated by means of the signal power (a) and three impulse equations (b–d) during 1 month of intense transport (July 2016). The signal produced by the flood event of 12 July 2016 is damped in a time series of impulse rates as it exceeds the different clipping thresholds. Rising impulse thresholds, bedload peaks are better represented but the time series of impulse rates are less sensitive to low-intensity signals: the lower cutoff limit (1 impulse) is 0.03 kg/min in (b), 0.5 kg/min in (c), and 3.25 kg/min in (d).

rates during large floods align well with values predicted using transport capacity equations, whereas bedload rates occurring during more frequent, "ordinary" competent flows are limited by sediment supply, that is, the quantity of sediment available for transport during such flows (Comiti et al., 2019; Lane et al., 2017; Recking, 2012). In a glacier-fed river, such as the Sulden, channel runoff is a function of both hydrological (precipitation) and meteorological (air temperature and solar radiation) variables during the entire year, because snowmelt and glacier-melt processes are driven by such variables (Engel, Penna, et al., 2019). However, different origins of runoff (rainfall events, snowmelt, and glacier melt) have been associated with different bedload supply levels and thus to extremely different bedload transport rates (Comiti et al., 2019; Mao et al., 2014). The use of bedload concentration permits

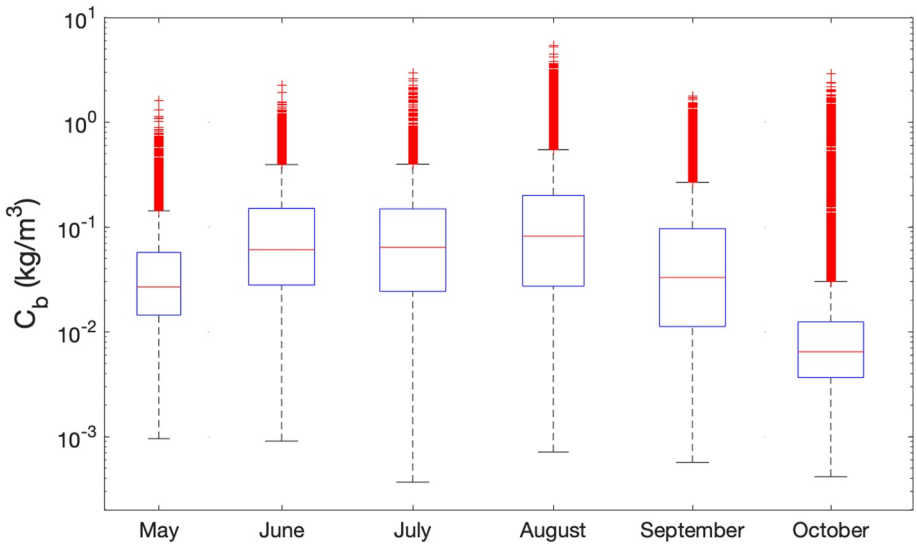

Figure 13. Bedload concentration measured at the Stilfserbrücke station from 2014 to 2020 grouped.

to analyze how factors other than water discharge—and thus different from transport capacity as long as the channel slope remains unchanged—may influence bedload transport rates. In particular, markedly different supply "regimes" have been associated with snowmelt and glacier-melt periods by Comiti et al. (2019). Similarly, Lenzi et al. (2004) normalized bedload volumes measured in the Rio Cordon station (Italy) by the associated (effective) runoff volumes, thereby demonstrating how sediment supply variations due to large flood events or inputs from tributaries dictate bedload export at the catchment scale. In a small glacier catchment (upper Saldur River, 20 km^2, 12% relative glacier area), the bedload concentration during the glacier-melt period was several orders of magnitude higher than during snowmelt (Comiti et al., 2019). Similar results—based on comparing bedload concentration—were found in a small glacier-fed stream of the Central Chilean Andes by Carrillo and Mao (2020). Remarkably, such a marked difference in the bedload concentration is not visible in the Sulden River (Figure 13), probably because our data were collected at the basin outlet, where the drainage area is almost an order of magnitude larger than the upper Saldur. Indeed, bedload sources in the Sulden basin are numerous, covering relatively large areas (including the channels itself) and not only related to glacial and proglacial areas (Buter et al., 2020) as was instead the case for the Saldur River. Nonetheless, the median bedload concentration in the Sulden River is likewise higher in July–August than in May–June and September–October, respectively (Figure 13). The important contribution of glacial sediments (i.e., fed by supra- and sub-glacial processes to the outflow stream) on bedload transport is supported by bedload sampling performed from 2015 to 2020 at the Sulden glacier snout (Engel, Coviello, et al., 2019). It is worth highlighting how unit bedload rates estimated in the Sulden River during intense glacier melt flows (about 11 kg m^{-1} min^{-1}) are slightly higher compared to those (about 8 kg m^{-1} min^{-1}) measured under similar hydrologic conditions in the Saldur River (Comiti et al., 2019), even though the unit stream power at such flows (400–500 W m^{-2}) is lower than at Sulden River (700–800 W m^{-2}). Both streams—at the monitored sections—feature comparable channel slope (4.7% Sulden vs. 6% Saldur) and relative glacier area (14% Sulden vs. 11% Saldur), but the Sulden is larger in terms of drainage area (130 vs. 19 km^2) and thus of glacial runoff.

We interpret the difference between snowmelt and glacier melt periods in terms of the bedload concentration measured at the monitoring station as the result of a complex chain of processes involving both the upper boundary conditions (i.e., glacial and proglacial sediment inputs) and the in-channel sediment storage, as already put forward by Comiti et al. (2019). Specifically, daily cycles of coarse sediment supply from the glacier trigger a cascading momentum transfer (Ancey et al., 2015; Kammerlander et al., 2017), which enhance bedload mobility of particles already present within the channel. Each coarse sediment particle released by the glaciers most likely reaches the monitoring station only after long times (weeks to months, if travel velocities are similar to those measured by Mao et al., 2017, in the Saldur River), but its momentum is effectively transferred downstream to the bed material temporarily stored in the channel.

Field evidence confirms that both glacial and proglacial sediment sources significantly contribute to the high bedload rate measured in the Sulden River in July and August, either during heatwaves or associated with intense

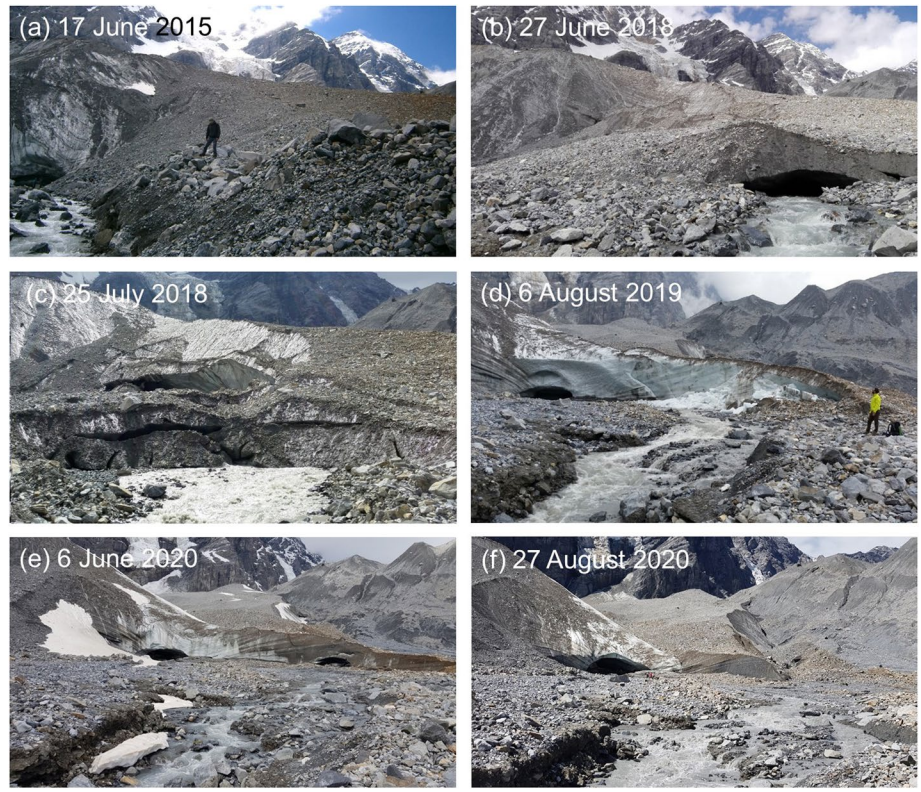

Figure 14. Evolution of Sulden glacier front from 2015 to 2020, the location of the site is indicated in Figure 1.

rainfall events that occurred in the investigated period (Figure 14). In 2017, for example, a new glacier mouth opened and created a new proglacial stream that quickly eroded the glacial forefields (Figure 14b), thereby sharply augmenting bedload supply to downstream reaches (Buter et al., 2022). In the following years, the glacier retreated by about 200 m producing remarkable geomorphic changes in the proglacial drainage network and leaving abundant loose sediments readily available for transport (Figures 14c–14f).

Even though basin-wide rainfall-related floods can transport a disproportionate share of the annual bedload yield in some specific years (see Section 3.2), glacier-melt runoff appears to have a dominant role in the long-term bedload transport in the Sulden River. This finding is supported by the magnitude-frequency analysis. The "most effective" discharge range for bedload (Figure 8b, from about 14 to 18 $m^3\ s^{-1}$) corresponds to the values reached during the most intense glacier melt periods (the red-shaded area in Figure 8b) with flow frequencies much higher—several times per year—than the 2–5 years in recurrence interval found for a nonglacial mountain stream (i.e., at Rio Cordon, Lenzi et al., 2006).

In contrast to what observed in the Rio Cordon—which features a step pool morphology—Bunte et al. (2014) argued that plane-bed, snowmelt-controlled streams with low sediment supply in forested Rocky Mountain watersheds may have effective discharges corresponding to much higher flows than bankfull flows. Our results from the magnitude-frequency analysis markedly contrast to both of these studies and show the dominant role of glacial runoff and proglacial sediment sources on bedload export, as preliminary observed by Comiti et al. (2019). The maximum of the E_Q curve (Figure 8) is likely due to the combination of the increase of water discharge due to glacier melt and the progressive activation of glacial (supra- and subglacial mostly) and proglacial sediment sources. Thus, the sediment export from the glacier dramatically increases during heat waves that typically occur in July and August.

The role of ordinary ($Q_{1.5}$) and less frequent floods (Q_{10}) is also visible in Figure 8 (second and third peaks of the E_Q curve, respectively), but their contribution to the long-term bedload export from the Sulden basin is definitely lower compared to the glacier-melt runoff. Such temperature-driven flow events will progressively lose their present dominance for bedload transport in the next decades as Sulden glaciers are rapidly retreating (Savi,

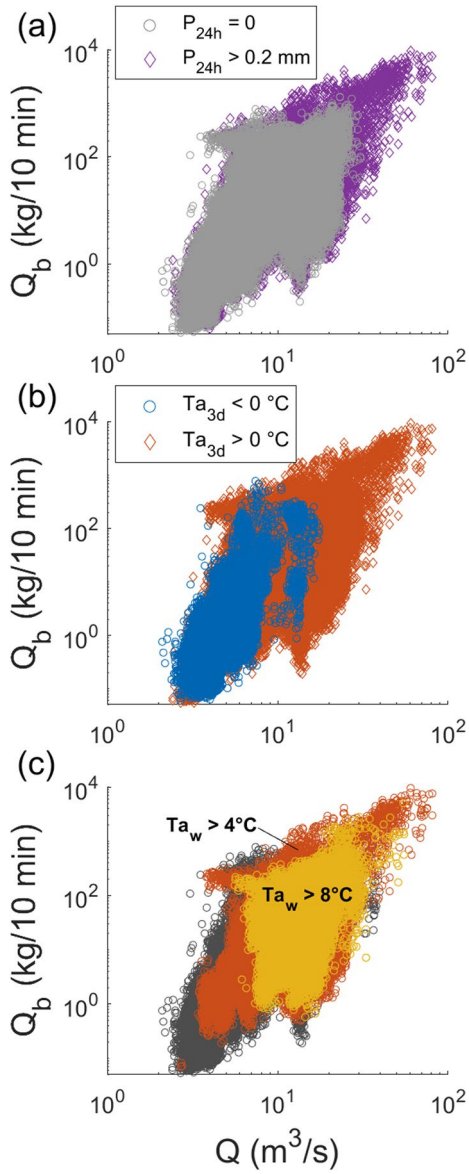

Figure 15. Bedload rate at the reference plate versus discharge calculated for all monitored periods and classified using three hydrometeorological parameters: the cumulated rainfall in the antecedent 24 hr (a), the mean air temperature of the previous 3 days (b), and the mean air temperature of the previous 7 days (c) measured at the Madritsch AWS. Dark gray points in (c) represent the complete data set, including points with $Ta_w < 4$°C. In some cases, points belonging to different runoff origins show similar values of T and P due to the co-occurrence of high temperatures and precipitation events.

Dinale, & Comiti, 2021). Then, rainfall-induced bedload events will likely become the dominant process driving bedload in the context of the ongoing climate warming. During the latest phase of deglaciation—with glacial sedimentary sources exhausted, stabilized, or disconnected from active processes of sediment transfer—bedload export is expected to decline due to the reduction of both sediment supply and runoff volumes (Antoniazza & Lane, 2021; Comiti et al., 2019; Li et al., 2021).

The current strong control of precipitation and air temperature on bedload transport is shown in Figure 15, where the whole bedload data set collected from 2014 to 2020 is analyzed in comparison with hydrometeorological parameters gathered at Madritsch AWS. In the figure, maximum bedload rates are classified based on the cumulated precipitation recorded in the previous 24 hr (P_{24h}) and on the mean air temperature of the previous 3 and 7 days, respectively, Ta_{3d} and Ta_w. The bedload load for different hydrometeorological conditions was calculated and compared with the total bedload yield of the analyzed period (7 years). This analysis shows that:

1. 50% of the total bedload load occurs with zero precipitation in the previous 24 hr (gray points in Figure 15a), highlighting the role of the glacier areas as sediment sources. The upper and the right limits of the distribution of bedload peak rates occurring with zero precipitation in the previous 24 hr (light gray points in Figure 15a) are 10^3 kg in 10 min and 30 m^3 s^{-1}, respectively;
2. the higher bedload rates (10^3–10^4 kg in 10 min) and the bedload concentration (5 kg m^{-3}) are associated with rainfall events that occurred in the antecedent 24 hr (Figure 15a), indicating that the largest bedload rates and concentrations are reached when sediment sources from a vast part of the basin are connected to the outlet, as argued by Buter et al. (2022);
3. most bedload transport is observed during the glacier melt period, when temperatures are above 0° for 3 consecutive days, which occur in July–August. In particular, more than 95% of the total bedload yield occurs with $Ta_{3d} > 0$°C (Figure 15b), whereas about 80% with $Ta_w > 4$°C (Figure 15c). Also, in the flow interval 14–18 m^3 s^{-1} (i.e., the main E_Q peak), 95% of bedload transport occurs with $Ta_{3d} > 0$°C and the 89% with $Ta_w > 4$°C.

The outcome of this analysis matches the results obtained by the magnitude-frequency analysis (Figure 8b) and highlights (a) the primary role of temperature in modulating glacier and snowmelt, thus driving the most bedload yield, and (b) the importance of intense rainfall events in generating bedload peak rates. This confirms the assumptions adopted in Buter et al. (2022) to analyze how the sediment connectivity varies in the Sulden river basin according to different hydrometeorological scenarios. These authors show how the functionally connected landforms greatly increase in number—and thus connected sediment sources increase in the area—when passing from "base" summer flows to heatwaves and then to heavy rainfall events occurring during or right after heatwaves.

4.3. Sources of Uncertainty and Research Perspectives

Seismic parameters that are representative of the energy transfer produced by particle impacts on the plate should be adopted for the calibration of geophone-plate data when the raw signal is available. Despite the significant advancements provided by the use of the signal power, the problem of the correct representation of peak bedload rates is probably not completely solved. During ordinary high-flow events (i.e., $Q_{1.5} = 40$ m^3 s^{-1}), part of the gravel fraction may travel at least intermittently as suspended load, not impacting on the plates and thus not

contributing to the signal generation. This process and the related bedload underestimation have been observed in other monitored streams (Wyss et al., 2016b) and are expected to be particularly pronounced at higher flow discharge (i.e., $Q_{10} = 73$ m^3 s^{-1}). In addition, bedload samples were collected at flows ranging from 6 to 21 m^3 s^{-1}, whereas peak discharge reached about 80 and 70 m^3 s^{-1} during 2014 and 2020 floods. Therefore, extrapolating the calibration relation to high flows (about Q_{10}) having sampled bedload only up to about 0.5 $Q_{1.5}$ brings in a significant uncertainty that can be reduced populating the bedload calibration curve with data collected at higher flow discharges. Finally, covering the entire cross section with geophone plates would reduce the uncertainty in the estimation of bedload yield due to lateral differences in transport rates.

Regarding the effect of the GSD on the geophone-plate signal, our findings show only a limited bedload coarsening for increasing water discharge within the sampled flow range, similar to what has been observed in other mountain streams (Rickenmann et al., 2012). In general, larger grain sizes tend to deliver more energy to the sensors (Turowski et al., 2015) and this may result in a nonlinear energy delivery from the flow to the plate when grain size distribution changes. The small variation of bedload grain size (both d_{50} and d_{90}) with increasing discharge illustrated by our data (Figure 5) well reflects what was observed in another glacier-fed river in the same region (Comiti et al., 2019). We attribute such gentle trends to a possible undersampling of the largest transported cobbles—due to the necessarily short sampling times at high flows—coupled to the relatively high mobility of coarse gravel and small cobbles at relatively small flows, typical of glacier-fed rivers (Mao et al., 2017). The characteristics of single impacts are needed to infer more accurate information about bedload GSD by differentiating impacts from small and large clasts. During intense transport periods, multiple impacts from grains of different sizes can occur at the same time and produce a complex seismic wave. Presently, a more accurate GSD discrimination based on geophone-plate data can be obtained only for controlled laboratory experiments (Nicollier et al., 2021; Wyss et al., 2016a).

5. Conclusions

In this study, we presented an original geophone-plate data set gathered in a glacier-fed Alpine river. We analyzed 7 years of bedload data at different temporal scales. We propose the signal power as a more effective signal metric to represent peak bedload rates than threshold-based impulses, which can underestimate the annual bedload yield by up to 20%. This allowed investigating the large variability of bedload rates and concentrations observed at the Sulden River. We found that air temperature is useful to identify periods of intense bedload transport, which is not only related to precipitation events but also to snowmelt and in particular to glacier melt. The bedload rate may vary up to four orders of magnitude for the same flow discharge, and bedload peak values are related to episodic summer rainstorm events superimposed on warm periods. Water discharge surely sets the maximum bedload fluxes possible in a given section but sediment supply—mostly coming from glacial and proglacial areas—dictates the actual transport rates in glacier-fed rivers during dry periods. In fact, maximum values of bedload concentration are reached in July and August, highlighting the control exerted by glacier melt on bedload yield. However, the two largest flood events occurred during the monitored period—due to intense rainfall storms—mobilized 30% and 70% of the annual bedload yields, respectively. This evidence has profound implications on how we should model future changes in glacier-fed rivers due to climate change. The results of this study add an additional knowledge tile in the understanding of how climate may control the sediment dynamics of a glaciered mountain basin.

Data Availability Statement

The geophone-plate data set (2014–2020) employed in this study can be accessed at: https://doi.org/10.5281/zenodo.7098023 (Coviello et al., 2022).

Acknowledgments
The research in the Sulden/Solda basin was supported by the AQUASED and GLORI projects (funded by the Autonomous Province of Bozen-Bolzano) and by the EFRE-FESR projects SEDIPLAN-i and -r. We are grateful to Roberto Dinale and Rudi Nadalet (Civil Protection Agency of the Autonomous Province of Bozen-Bolzano) and to the staff of the Meteorological and Hydrological Office of the Autonomous Province of Bozen-Bolzano for providing hydrometeorological data gathered in the Sulden basin. The design of the geophone-plate monitoring station of Stilfserbrücke—Ponte Stelvio benefited from advice by Dieter Rickenmann. We thank many colleagues and students for their support in bedload sampling activities at Sulden, in particular Ricardo Carrillo, Christian Kofler, Federica Minotti, Francesca Minute, Shusuke Miyata, Matteo Roverato, and Vittoria Scorpio. We would also like to thank K. Bunte, an anonymous reviewer, and the Editor E. Wohl for their thoughtful and constructive revisions of this paper. Open Access Funding provided by Consiglio Nazionale delle Ricerche within the CRUI-CARE Agreement.

References

Ancey, C., Bohorquez, P., & Heyman, J. (2015). Stochastic interpretation of the advection-diffusion equation and its relevance to bed load transport. *Journal of Geophysical Research: Earth Surface*, *120*(12), 2529–2551. https://doi.org/10.1002/2014JF003421

Antoniazza, G., & Lane, S. N. (2021). Sediment yield over glacial cycles: A conceptual model. *Progress in Physical Geography*, *45*(6), 842–865. https://doi.org/10.1177/0309133321997292

Arattano, M., Abancó, C., Coviello, V., & Hürlimann, M. (2014). Processing the ground vibration signal produced by debris flows: The methods of amplitude and impulses compared. *Computers & Geosciences*, *73*, 17–27. https://doi.org/10.1016/j.cageo.2014.08.005

Autonomous Province of Bozen/Bolzano. (2017). Catasto dei ghiacciai dell'Alto Adige 2016/17 [Internal report]. Ufficio Idrologia e Dighe.
Baewert, H., & Morche, D. (2014). Coarse sediment dynamics in a proglacial fluvial system (Fagge River, Tyrol). *Geomorphology*, *218*, 88–97. https://doi.org/10.1016/j.geomorph.2013.10.021
Bagnold, R. A. (1977). Bed load transport by natural rivers. *Water Resources Research*, *13*(2), 303–312. https://doi.org/10.1029/WR013i002p00303
Barry, J. J., Buffington, J. M., & King, J. G. (2004). A general power equation for predicting bed load transport rates in gravel bed rivers. *Water Resources Research*, *40*(10), 1–22. https://doi.org/10.1029/2004WR003190
Beylich, A. A., & Laute, K. (2015). Sediment sources, spatiotemporal variability and rates of fluvial bedload transport in glacier-connected steep mountain valleys in Western Norway (Erdalen and Bødalen drainage basins). *Geomorphology*, *228*, 552–567. https://doi.org/10.1016/j.geomorph.2014.10.018
Bogen, J., Xu, M., & Kennie, P. (2015). The impact of pro-glacial lakes on downstream sediment delivery in Norway. *Earth Surface Processes and Landforms*, *40*(7), 942–952. https://doi.org/10.1002/esp.3669
Borga, M., Stoffel, M., Marchi, L., Marra, F., & Jakob, M. (2014). Hydrogeomorphic response to extreme rainfall in headwater systems: Flash floods and debris flows. *Journal of Hydrology*, *518*(PB), 194–205. https://doi.org/10.1016/j.jhydrol.2014.05.022
Bunte, K., Abt, S. R., Swingle, K. W., & Cenderelli, D. A. (2014). Effective discharge in Rocky Mountain headwater streams. *Journal of Hydrology*, *519*(PB), 2136–2147. https://doi.org/10.1016/j.jhydrol.2014.09.080
Buter, A., Heckmann, T., Filisetti, L., Savi, S., Mao, L., Gems, B., & Comiti, F. (2022). Effects of catchment characteristics and hydro-meteorological scenarios on sediment connectivity in glacierised catchments. *Geomorphology*, *402*, 108128. https://doi.org/10.1016/j.geomorph.2022.108128
Buter, A., Spitzer, A., Comiti, F., & Heckmann, T. (2020). Geomorphology of the Sulden River basin (Italian Alps) with a focus on sediment connectivity. *Journal of Maps*, *16*(2), 890–901. https://doi.org/10.1080/17445647.2020.1841036
Carrillo, R., & Mao, L. (2020). Coupling sediment transport dynamics with sediment and discharge sources in a glacial Andean basin. *Water (Switzerland)*, *12*(12), 1–25. https://doi.org/10.3390/w12123452
Carrivick, J. L., & Tweed, F. S. (2021). Deglaciation controls on sediment yield: Towards capturing spatio-temporal variability. *Earth-Science Reviews*, *221*(June), 103809. https://doi.org/10.1016/j.earscirev.2021.103809
Comiti, F., & Mao, L. (2012). Recent advances in the dynamics of steep channels. *Gravel-Bed Rivers: Processes Tools, Environment*, 351–377. https://doi.org/10.1002/9781119952497.ch26
Comiti, F., Mao, L., Penna, D., Dell'Agnese, A., Engel, M., Rathburn, S., & Cavalli, M. (2019). Glacier melt runoff controls bedload transport in Alpine catchments. *Earth and Planetary Science Letters*, *520*, 77–86. https://doi.org/10.1016/j.epsl.2019.05.031
Coviello, V., Capra, L., Vázquez, R., & Márquez-Ramírez, V. H. (2018). Seismic characterization of hyperconcentrated flows in a volcanic environment. *Earth Surface Processes and Landforms*, *43*(10), 2219–2231. https://doi.org/10.1002/esp.4387
Coviello, V., Vignoli, G., Bertoldi, W., Simoni, S., & Comiti, F. (2022). Geophone plate data from the Sulden/Solda basin (South Tyrol, Italy) 2014-2020 [Dataset]. Zenodo. https://doi.org/10.5281/zenodo.7098023
Delaney, I., Bauder, A., Werder, M. A., & Farinotti, D. (2018). Regional and annual variability in subglacial sediment transport by water for two glaciers in the Swiss Alps. *Frontiers of Earth Science*, *6*(October), 1–17. https://doi.org/10.3389/feart.2018.00175
Einstein, H. A. (1950). *The bed-load function for sediment transportation in open channel flows*. US Department of Agriculture.
Engel, M., Coviello, V., Andreoli, A., Buter, A., Kofler, C., Scorpio, V., et al. (2019). How does the presence of debris-cover on a glacier influence hydro-sedimentary dynamics? A comparison study from two proglacial streams in the Sulden catchment (Eastern Italian Alp s). In *EGU general assembly*, (Vol. 21), EGU2019-13295. Universitat innsbruck.
Engel, M., Penna, D., Bertoldi, G., Vignoli, G., Tirler, W., & Comiti, F. (2019). Controls on spatial and temporal variability in streamflow and hydrochemistry in a glacierized catchment. *Hydrology and Earth System Sciences*, *23*(4), 2041–2063. https://doi.org/10.5194/hess-23-2041-2019
Etzelmüller, B., & Frauenfelder, R. (2009). Factors controlling the distribution of mountain permafrost in the northern hemisphere and their influence on sediment transfer factors controlling the distribution of mountain permafrost in the northern hemisphere and their influence on sediment transfer. *Arctic, Antarctic, and Alpine Research*, *41*(1), 48–58. https://doi.org/10.1657/1938-4246(08-026)
Gimbert, F., Tsai, V. C., & Lamb, M. P. (2014). A physical model for seismic noise generation by turbulent flow in rivers. *Journal of Geophysical Research: Earth Surface*, *119*(10), 2209–2238. https://doi.org/10.1002/2014JF003201
Habersack, H., Kreisler, A., Rindler, R., Aigner, J., Seitz, H., Liedermann, M., & Laronne, J. B. (2017). Integrated automatic and continuous bedload monitoring in gravel bed rivers. *Geomorphology*, *291*, 80–93. https://doi.org/10.1016/j.geomorph.2016.10.020
Harrison, L. R., Legleiter, C. J., Wydzga, M. A., & Dunne, T. (2011). Channel dynamics and habitat development in a meandering, gravel bed river. *Water Resources Research*, *47*(4), 1–21. https://doi.org/10.1029/2009WR008926
Kammerlander, J., Gems, B., Kößler, D., & Aufleger, M. (2017). Effect of bed load supply on sediment transport in mountain streams. *International Journal of Sediment Research*, *32*(2), 240–252. https://doi.org/10.1016/j.ijsrc.2017.03.004
Kociuba, W. (2017). Determination of the bedload transport rate in a small proglacial High Arctic stream using direct, semi-continuous measurement. *Geomorphology*, *287*, 101–115. https://doi.org/10.1016/j.geomorph.2016.10.001
Kofler, C., Mair, V., Gruber, S., Todisco, M. C., Nettleton, I., Steger, S., et al. (2021). When do rock glacier fronts fail? Insights from two case studies in South Tyrol (Italian Alps). *Earth Surface Processes and Landforms*, *46*(7), 1311–1327. https://doi.org/10.1002/ESP.5099
Lane, S. N., Bakker, M., Gabbud, C., Micheletti, N., & Saugy, J. (2017). Sediment export, transient landscape response and catchment-scale connectivity following rapid climate warming and Alpine glacier recession. *Geomorphology*, *277*, 210–227. https://doi.org/10.1016/j.geomorph.2016.02.015
Lenzi, M. A., Mao, L., & Comiti, F. (2004). Magnitude-frequency analysis of bed load data in an Alpine boulder bed stream. *Water Resources Research*, *40*(7), 1–12. https://doi.org/10.1029/2003WR002961
Lenzi, M. A., Mao, L., & Comiti, F. (2006). Effective discharge for sediment transport in a mountain river: Computational approaches and geomorphic effectiveness. *Journal of Hydrology*, *326*(1–4), 257–276. https://doi.org/10.1016/j.jhydrol.2005.10.031
Li, D., Overeem, I., Kettner, A. J., Zhou, Y., & Lu, X. (2021). Air temperature regulates erodible landscape, water, and sediment fluxes in the permafrost-dominated catchment on the Tibetan plateau. *Water Resources Research*, *57*(2), 1–14. https://doi.org/10.1029/2020WR028193
Mao, L. (2012). The effect of hydrographs on bed load transport and bed sediment spatial arrangement. *Journal of Geophysical Research*, *117*(July), 1–16. https://doi.org/10.1029/2012JF002428
Mao, L., Comiti, F., Carrillo, R., & Penna, D. (2019). Sediment transport in proglacial rivers. In T. Heckmann, & D. Morche (Eds.), *Geomorphology of Proglacial Systems. Landform and Sediment Dynamics in Recently Deglaciated Alpine Landscapes* (pp. 199–217). Springer International Publishing.
Mao, L., Dell'Agnese, A., & Comiti, F. (2017). Sediment motion and velocity in a glacier-fed stream. *Geomorphology*, *291*, 69–79. https://doi.org/10.1016/j.geomorph.2016.09.008
Mao, L., Dell'Agnese, A., Huincache, C., Penna, D., Engel, M., Niedrist, G., & Comiti, F. (2014). Bedload hysteresis in a glacier-fed mountain river. *Earth Surface Processes and Landforms*, *39*(7), 964–976. https://doi.org/10.1002/esp.3563

Meyer-Peter, E., & Müller, R. (1948). Formulas for bed-load transport. In *IAHSR 2nd meeting, stockholm, appendix 2*. IAHR. [online] Retrieved from https://repository.tudelft.nl/islandora/object/uuid%3A4fda9b61-be28-4703-ab06-43cdc2a21bd7

Mizuyama, T., Fujita, M., & Nonaka, M. (2003). *Measurement of bed load with the use of hydrophones in mountain torrents* (pp. 222–227). IAHS-AISH Publications.

Nicollier, T., Rickenmann, D., & Hartlieb, A. (2021). Field and flume measurements with the impact plate: Effect of bedload grain-size distribution on signal response. *Earth Surface Processes and Landforms*, *46*(8), 1504–1520. https://doi.org/10.1002/esp.5117

Perolo, P., Bakker, M., Gabbud, C., Moradi, G., Rennie, C., & Lane, S. N. (2019). Subglacial sediment production and snout marginal ice uplift during the late ablation season of a temperate valley glacier. *Earth Surface Processes and Landforms*, *44*(5), 1117–1136. https://doi.org/10.1002/esp.4562

Raymond Pralong, M., Turowski, J. M., Rickenmann, D., & Zappa, M. (2015). Climate change impacts on bedload transport in alpine drainage basins with hydropower exploitation. *Earth Surface Processes and Landforms*, *40*(12), 1587–1599. https://doi.org/10.1002/esp.3737

Recking, A. (2012). Influence of sediment supply on mountain streams bedload transport. *Geomorphology*, *175–176*, 139–150. https://doi.org/10.1016/j.geomorph.2012.07.005

Rickenmann, D. (2001). Comparison of bed load transport in torrents and gravel bed streams. *Water Resources Research*, *37*(12), 3295–3305. https://doi.org/10.1029/2001WR000319

Rickenmann, D. (2018). Variability of bed load transport during six summers of continuous measurements in two Austrian mountain streams (Fischbach and Ruetz). *Water Resources Research*, *54*(1), 107–131. https://doi.org/10.1002/2017WR021376

Rickenmann, D., Badoux, A., & Hunzinger, L. (2016). Significance of sediment transport processes during piedmont floods: The 2005 flood events in Switzerland. *Earth Surface Processes and Landforms*, *41*(2), 224–230. https://doi.org/10.1002/esp.3835

Rickenmann, D., Turowski, J. M., Fritschi, B., Klaiber, A., & Ludwig, A. (2012). Bedload transport measurements at the Erlenbach stream with geophones and automated basket samplers. *Earth Surface Processes and Landforms*, *37*(9), 1000–1011. https://doi.org/10.1002/esp.3225

Rickenmann, D., Turowski, J. M., Fritschi, B., Wyss, C. R., Laronne, J., Barzilai, R., et al. (2014). Bedload transport measurements with impact plate geophones: Comparison of sensor calibration in different gravel-bed streams. *Earth Surface Processes and Landforms*, *39*(7), 928–942. https://doi.org/10.1002/esp.3499

Rinaldi, M., Surian, N., Comiti, F., & Bussettini, M. (2015). A methodological framework for hydromorphological assessment, analysis and monitoring (IDRAIM) aimed at promoting integrated river management. *Geomorphology*, *251*, 122–136. https://doi.org/10.1016/j.geomorph.2015.05.010

Savi, S., Comiti, F., & Strecker, M. R. (2021). Pronounced increase in slope instability linked to global warming: A case study from the eastern European Alps. *Earth Surface Processes and Landforms*, *46*(7), 1–20. https://doi.org/10.1002/esp.5100

Savi, S., Dinale, R., & Comiti, F. (2021). The sulden/solda glacier (Eastern Italian Alps): Fluctuations, dynamics, and topographic control over the last 200 years. *Geografia Fisica e Dinamica Quaternaria*, *44*, 15–30. https://doi.org/10.4461/GFDQ.2021.44.2

Schneider, J. M., Rickenmann, D., Turowski, J. M., Schmid, B., & Kirchner, J. W. (2016). Bed load transport in a very steep mountain stream (Riedbach, Switzerland): Measurement and prediction. *Water Resources Research*, *52*(12), 9522–9541. https://doi.org/10.1002/2016WR019308

Turowski, J. M., Badoux, A., & Rickenmann, D. (2011). Start and end of bedload transport in gravel-bed streams. *Geophysical Research Letters*, *38*(4), 1–5. https://doi.org/10.1029/2010GL046558

Turowski, J. M., Wyss, C. R., & Beer, A. R. (2015). Grain size effects on energy delivery to the streambed and links to bedrock erosion. *Geophysical Research Letters*, *42*(6), 1775–1780. https://doi.org/10.1002/2015GL063159

Vignoli, G., Simoni, S., Comiti, F., Agnese, A. D., & Bertoldi, W. (2016). Monitoring sediment fluxes in Alpine rivers: The AQUASED project (pp. 426–433). Data Acquisition and Modelling (Monitoring, Processes, Technologies, Models).

Wolman, M. G., & Miller, J. P. (1960). Magnitude and frequency of forces in geomorphic processes. *The Journal of Geology*, *68*(1), 54–74. https://doi.org/10.1086/626637

Wyss, C. R., Rickenmann, D., Fritschi, B., Turowski, J. M., Weitbrecht, V., & Boes, R. M. (2016a). Laboratory flume experiments with the Swiss plate geophone bed load monitoring system: 1. Impulse counts and particle size identification. *Water Resources Research*, *52*(10), 7744–7759. https://doi.org/10.1002/2015WR018555

Wyss, C. R., Rickenmann, D., Fritschi, B., Turowski, J. M., Weitbrecht, V., Travaglini, E., et al. (2016b). Laboratory flume experiments with the Swiss plate geophone bed loadmonitoring system: 2. Application to field sites with direct bed load samples. *Water Resources Research*, *52*(10), 7760–7778. https://doi.org/10.1002/2016WR019283